



Quantifying grid flexibility provision of virtual vehicle-to-vehicle energy sharing using statistically similar networks[☆]

Wei Gan, Yue Zhou, Jianzhong Wu^{*}

School of Engineering, Cardiff University, Cardiff CF24 3AA, UK

HIGHLIGHTS

- A virtual vehicle-to-vehicle energy sharing framework is firstly proposed.
- A statistically similar network method is implemented and enhanced.
- A bottom-up model of electric vehicles travel and plugging patterns is introduced.
- Flexibility provision from virtual vehicle-to-vehicle is quantified.

ARTICLE INFO

Keywords:

Electric vehicles integration
Vehicle-to-vehicle energy sharing
Bottom-up modeling
Flexibility provision
Statistically similar networks

ABSTRACT

The rapid rise in electric vehicle (EV) adoption presents significant capacity challenges for power grids, but with effective charging management, EVs can also serve as flexible resources, underscoring the need for relevant innovative solutions. This paper proposes a virtual vehicle-to-vehicle (V-V2V) framework, enabling EVs to share energy with each other, either at public charging stations or home, as long as they are connected to the same distribution network. The framework eliminates the need for physical proximity and peer-to-peer matching seen in traditional V2V, enhancing grid flexibility and reducing capacity pressures by harmonizing EV charging with other demands and photovoltaic generation. To quantify the flexibility provision of the V-V2V framework, this paper implements and enhances the statistically similar networks method, where simulations are based on generated networks that share similar electrical and topological characteristics, rather than relying on a single network. Using graph theory, the method preserves statistical similarity in both electrical and topological features, along with their internal correlations, ensuring the practicality of the network simulations. To improve flexibility quantification accuracy, this paper introduces a bottom-up, high-granularity model of EV travel and plugging patterns that accounts for diverse user archetypes. Monte Carlo simulations are employed to provide a detailed analysis of travel and charging behaviors by categorizing EV users. The effectiveness of the proposed method is tested through numerical results using real-world UK distribution networks.

1. Introduction

Amid the global shift toward a low-carbon economy and the concerted efforts by nations to achieve net-zero emissions, the transportation sector is experiencing rapid decarbonization and electrification [1]. This transformation is particularly evident in the aggressive adoption of electric vehicles (EVs), driven by policy mandates [2], technological advancements [3], and a growing consumer preference for sustainability [4]. In the UK, 80 % of new cars sold are projected to be zero-emission by 2030, rising to 100 % by 2035. The cumulative number

of EVs is expected to surpass 15 million by 2035 and double to 30 million by 2050 [5]. Globally, nearly 14 million new EVs were registered in 2023, bringing the total number of EVs on the road to 40 million. This number is projected to grow to 250 million by 2030 and 525 million by 2035, with more than one in four vehicles expected to be electric. The global EV stock is anticipated to grow at an average annual rate of 23 % from 2023 to 2035 [6].

Despite being widely recognized as low-carbon and clean transportation solutions with numerous benefits, EVs also introduce significant challenges for the power distribution network. The integration of EVs can alter load profiles, strain the capacity of distribution network

[☆] This article is part of a Special issue entitled: 'Low-Carbon Transport(Wen-Long Shang)' published in Applied Energy.

^{*} Corresponding author.

E-mail address: WuJ5@cardiff.ac.uk (J. Wu).

Nomenclature	
Indices and Sets	
i, ij, t	Indices of nodes, lines, and hours
$O(m)$	Index of public-charged EVs at the m -th charging point in a public parking lot, which varies across different scenarios and dates
$\Omega_{sub}, \Omega_{home}, \Omega_{public}$	Set of nodes with substations, home-charging chargers, and public parking lots
$ED(i), ST(i)$	Set of lines ending at node i and starting at node i
Parameters	
$\rho_t^{buy}, \rho_t^{sell}$	Electricity purchase and sell prices when trading with the utility company during hour t
$Asset_{ij}$	Asset value (i.e., investment cost) of line ij
$\overline{\Delta HR}_{ij}$	Max value for each segment, where the headroom rate of line ij is divided into K segments
$Slope_{ij,k}$	Slope of the piecewise linear APV_{ij} - HR_{ij} function at segment k
$Asset_i$	Asset value of the substation at node i
$\overline{\Delta HR}_i$	Max value for each segment, where the headroom rate of the substation at node i is divided into K segments
$Slope_{i,k}$	Slope of the piecewise linear APV_i - HR_i function at segment k
$Asset_i^{EVhome}$	Battery asset value of the home-charged EV at node i
\bar{E}_i^{EVhome}	Battery energy capacity of the home-charged EV at node i
$\bar{P}_i^{Homecharger}$	Max charging power of the home-charged EV at node i
$SOC_i^{arr}, SOC_i^{Nextdep}$	Arrival and departure SOC of the home-charged EV at node i
$t_i^{arr}, t_i^{Nextdep}$	Arrival and departure times of the home-charged EV at node i
$SOC_i^{threshold}$	SOC threshold for home-charged EV at node i to start charging (i.e., EV user will charge when SOC falls below this value)
$Asset_{i,o(m)}^{EVpub}$	Battery asset value of the public-charged EV at the m -th charging point in the public parking lot at node i
$\bar{E}_{i,o(m)}^{EVpub}$	Battery capacity in kWh of the public-charged EV at the m -th charging point in the public parking lot at node i
$\bar{P}_{i,m}^{Pubcharger}$	Max charging power of the m -th charging point in the public parking lot at node i
$SOC_{i,o(m)}^{arr}, SOC_{i,o(m)}^{Nextdep}$	Arrival and departure SOC of the public-charged EV at the m -th charging point in the public parking lot at node i
$t_{i,o(m)}^{arr}, t_{i,o(m)}^{Nextdep}$	Arrival and departure times of the public-charged EV at the m -th charging point in the public parking lot at node i
η	Charging and discharging efficiency of the EV battery
$PD_{i,t}^{nonEV}, QD_{i,t}^{nonEV}$	Active and reactive non-EV loads of the household at node i (non-EV loads include lighting, household appliances, and heating/cooling loads)
$\overline{PV}_{i,t}$	Max PV generation power at node i during hour t
R_{ij}, X_{ij}	Resistance and reactance of line ij
$\overline{SL}_{ij}, \overline{S}_i$	Capacity of line ij and the substation at node i
$\underline{U}, \overline{U}$	Lower and upper voltage limits
Variables	
P_t^{buy}, P_t^{sell}	Electricity bought from and sold to utility company during hour t
y_{ij}, y_i	Binary variables indicating the expansion planning status of line ij and the substation at node i
$PD_{i,t}^{EVhome}, PC_{i,t}^{EVhome}$	Discharging power and charging power of the home-charged EV at node i during hour t
$P_{i,t}^{EVhome}, E_{i,t}^{EVhome}$	Power injection and stored energy of the home-charged EV at node i during hour t
$PD_{i,m,t}^{EVpub}, PC_{i,m,t}^{EVpub}$	Discharging power and charging power of the m -th charging point in the public parking lot at node i during hour t
$P_{i,m,t}^{EVpub}$	Power injection of the m -th charging point in the public parking lot at node i during hour t
$E_{i,o(m),t}^{EVpub}$	Stored energy of the public-charged EV at the m -th charging point in the public parking lot at node i during hour t
APV_{ij}	APV of line ij
$HR_{ij}, \Delta HR_{ij,k}$	Headroom rate of line ij and the k -th segmental headroom rate value, where each segment is defined as the headroom rate of line ij divided into K segments
$SL_{ij}^{Peakflow}$	The peak apparent power flow of line ij during the entire simulation period
$PL_{ij,t}, QL_{ij,t}$	Active power and reactive power of line ij during hour t
APV_i	APV of the substation at node i
$HR_i, \Delta HR_{i,k}$	Headroom rate of the substation at node i and the k -th segmental headroom rate value, where each segment is defined as the headroom rate of the substation at node i divided into K segments
$S_i^{Peakflow}$	The peak apparent power flow of the substation at node i during the entire simulation period
$P_{i,t}^{sub}, Q_{i,t}^{sub}$	Active power and reactive power of the substation at node i during hour t
$PV_{i,t}$	Actual PV generation power at node i during hour t
$P_{i,t}^{in}, P_{i,t}^{out}$	Power injection and output at node i during hour t
$U_{i,t}, U_{j,t}$	Voltage at node i and node j during hour t

components, and result in voltage and frequency imbalances, excessive harmonic injection, power losses, and grid instability [7,8]. One of the most pressing concerns is the uncontrolled charging of EVs during peak hours, which places significant stress on the grid, given its limited capacity [9]. Moreover, the existing distribution infrastructure was not originally designed to accommodate the substantial additional load from EVs, which could result in overloading, connection queues, and network bottlenecks that hinder the integration of new EVs [10,11].

In response to these challenges, research and innovation have focused on developing EV charging management strategies. Smart charge, as a key approach, optimizes charging times by shifting EV charging from peak evening hours to off-peak periods, such as early morning, when demand is lower [12]. This can be supported by dynamic

pricing models that incentivize users to adjust their charging behavior, flattening demand curves and reducing grid stress. Furthermore, smart charge can be coordinated with photovoltaic (PV) systems, aligning EV charging times with peak PV output [13,14]. This strategy has gained traction and is being implemented by energy suppliers. EV-specific tariffs offering reduced rates for off-peak charging are increasingly being used to encourage grid-friendly charging patterns [15,16]. However, while these initiatives play a crucial role in harmonizing EV charging with grid capacity, they are only one aspect of the broader grid-interactive potential of EVs.

Beyond simple demand shifting through smart charge, the integration of EVs as active grid assets introduces a deeper synergy between transportation electrification and power system operations. In this

context, vehicle-to-grid (V2G) technology is a promising innovation that enables EVs to discharge energy back to the grid, thereby enhancing grid flexibility. As illustrated in Fig. 1, grid flexibility refers to the capability of flexible resources within the power grid to swiftly adjust their power output—either increasing or decreasing—in response to uncertain changes in generation, demand, network conditions or price signals of the bulk power grid. Unlocking the V2G potential of EVs allows them to actively contribute to grid flexibility, enabling participation in ancillary services such as peak shaving, load balancing, and emergency backup [17,18]. Consequently, leveraging V2G not only enhances grid flexibility but also creates new revenue opportunities for EV owners [19–21]. However, despite promising prospects, the real-world effectiveness of V2G in alleviating grid capacity pressures and optimising charging costs remains suboptimal, largely due to regulatory or market barriers and the unpredictability of user charging behavior [22,23].

At the low-voltage distribution level, EV users typically respond to economic signals, primarily electricity prices, when making charging and discharging decisions [24]. However, relying solely on price signals to influence user behavior has its limitations. EV users tend to prioritise immediate economic gains over grid benefits, such as reducing capacity pressures. In regions where feed-in tariffs offer low compensation for returning energy to the grid, users are discouraged from discharging their EVs, particularly due to concerns over battery degradation [25]. Conversely, in some markets, higher feed-in rates can lead to adverse effects, such as the simultaneous discharging of multiple EVs during off-peak periods, inadvertently creating new peak load challenges and exacerbating network congestion [26]. Therefore, there is a need for mechanisms that effectively harness the battery storage capacity of EVs to benefit both users and grid operations, particularly in mitigating grid capacity pressures.

In contrast to V2G, which focuses on interactions between the grid and EVs, vehicle-to-vehicle (V2V) technology offers an alternative solution for meeting EV charging needs. V2V allows EV owners with surplus energy to sell it to other EVs, helping to alleviate energy demand [27,28]. For EVs in need of energy, participation in a V2V framework is driven by their charging requirements. Meanwhile, EVs providing energy are motivated by financial incentives or mutual benefit, supplying energy with the expectation of compensation or future support [29,30]. However, traditional V2V requires substantial time commitments from both energy providers and recipients, as they need to be physically present or available during the energy exchange process. This limitation hinders large-scale adoption, making V2V more suitable for emergency situations, such as when an EV is low on battery and cannot reach a charging station, rather than for everyday use.

In response to these limitations, this paper introduces a virtual vehicle-to-vehicle energy sharing (V-V2V) framework, an innovative system where grid-connected EVs can share energy via the distribution network. Within this framework, two EVs at different locations on the

grid—one discharging and the other charging—participate in a virtual energy exchange, with the grid facilitating the transaction as if the EVs were directly sharing energy. Compared to the traditional V2V, V-V2V offers several key advantages: 1) EVs connected to the same distribution network can share energy without being physically co-located, and users do not have to wait for the energy transfer to finish; 2) traditional V2V is limited to one-to-one transactions, while V-V2V enables one-to-many or many-to-many exchanges; 3) V-V2V not only provides economic benefits to users but also creates an aggregation effect, improving grid flexibility and alleviating grid capacity pressures.

In addition to proposing the V-V2V framework, this paper aims to quantify its capability on grid flexibility provision, with a particular focus on mitigating grid capacity pressures. The key contributions are as follows:

- 1) This paper firstly proposes the V-V2V framework, enabling EVs to share energy with each other regardless of their location at public charging stations or home, as long as they are connected to the same distribution network. Unlike traditional V2V energy sharing, the proposed V-V2V framework eliminates the need for physical proximity and peer-to-peer matching. This approach not only maximizes the benefits of V2G technology by providing economic advantages to EV users, but more importantly, it enhances grid flexibility—mitigating grid capacity pressures by harmonizing EV charging with other demands as well as photovoltaic generation.
- 2) To quantify the flexibility provision from the proposed V-V2V framework, this paper implements and enhances statistically similar networks, using a set of generated networks that share statistically similar electrical and topological characteristics, rather than relying on a single network. This approach ensures more robust and statistically significant findings, as analyses based on a single network may not generalize well and could lead to substantial differences in other networks. Using graph theory, the method developed here preserves statistical similarity in both electrical and topological features, along with their internal correlations, ensuring the generated networks are practical and avoid mismatches.
- 3) To achieve more accurate and meaningful flexibility quantification, this paper introduces a bottom-up, high-granularity model of EV travel and plugging patterns that accounts for diverse EV user archetypes. With limited data, traditional models rely on aggregated probabilistic functions without distinguishing between user types (e.g., retirees, professionals, families with two EVs), which reduces the precision of charging simulations and flexibility quantification. This study employs bottom-up Monte Carlo simulations, which model individual user behavior through categorized probabilistic scenarios, to provide a more detailed and accurate analysis of travel and charging patterns by categorizing EV users in greater detail.

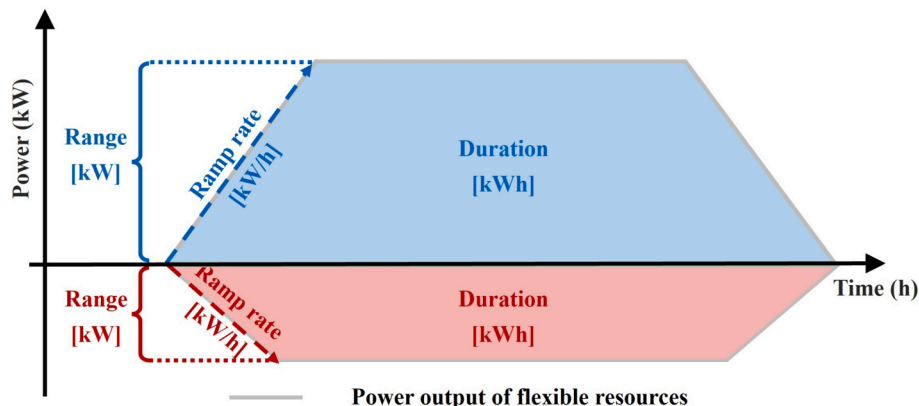


Fig. 1. Illustration of grid flexibility provision of flexible resources such as EVs.

The remainder of the paper is organized as follows. Section 2 presents the V-V2V energy sharing framework. Section 3 details the bottom-up, high-granularity EV travel and plugging patterns modeling, considering diverse EV user archetypes. Section 4 focuses on modeling V-V2V with grid flexibility provision. In Section 5, the statistically similar network-based method for quantifying grid flexibility is explained in detail. Section 6 applies and validates the proposed framework and method using real UK distribution networks. Conclusions are drawn in Section 7.

2. V-V2V Energy Sharing Framework

This paper introduces the innovative concept of V-V2V Energy Sharing, which differs from traditional methods where EVs share battery power via physical charging cables. Instead, this approach leverages the public power distribution network for connection. While the EVs are not directly connected by a single cable, they are linked through the public network, enabling one EV to discharge while another charges. This effectively creates a virtual energy-sharing mechanism, simulating a direct V2V energy exchange. Unlike conventional direct V2V energy sharing, which is restricted by the geographical proximity of the vehicles and can only occur on a one-to-one basis, the V-V2V approach enables energy sharing among all EVs connected to the network within a community, including both home-charged and public-charged EVs. As illustrated in Fig. 2, in a community powered by a low-voltage substation, various EVs are connected via the public distribution network. Additionally, V2V wireless communication is employed to coordinate the V-V2V process, allowing for dynamic adjustment of charging and discharging times and quantities across different EVs.

Implementing V-V2V requires only minor additional hardware and software enhancements, making it a cost-effective solution relative to its benefits. Most modern EVs are already equipped with communication modules (Wi-Fi, 4G/5G), eliminating the need for major modifications to individual vehicles. However, to enable coordinated energy exchange, a centralized coordination unit may be required within the public power network to match energy demand and supply among EVs. On the software side, a lightweight energy management platform can be seamlessly integrated into existing smart charge and V2G frameworks, enabling real-time scheduling of charging and discharging between vehicles at minimal cost. Given the benefits of V-V2V in lowering energy costs and enhancing grid flexibility, the modest investment in V-V2V is well justified by its substantial long-term advantages.

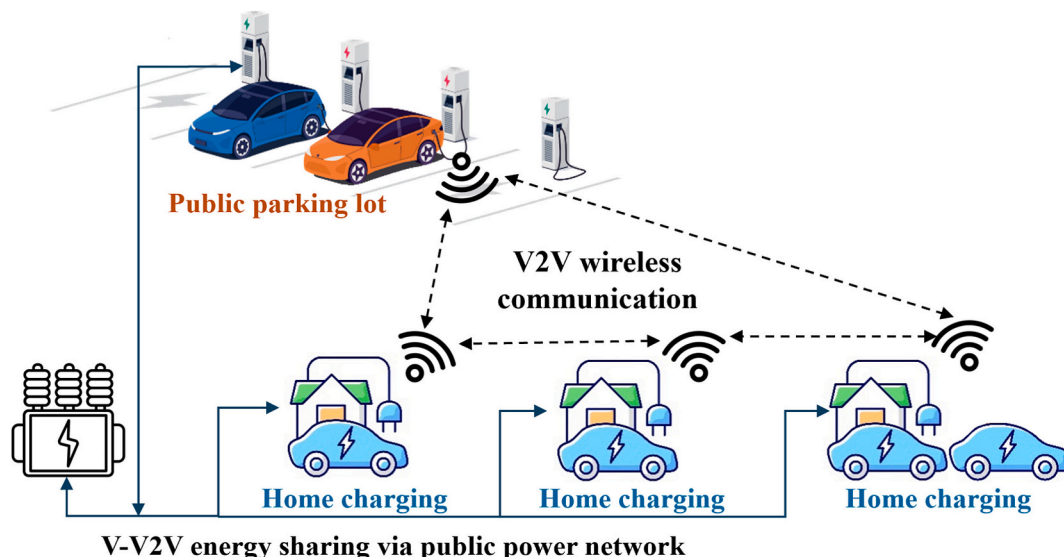


Fig. 2. V-V2V energy sharing framework.

3. Bottom-up High-Granularity Modeling of EV Travel and Charging Patterns

A key innovation of this paper is the proposed V-V2V architecture, along with the introduction and enhancement of a statistically similar network method to assess EV grid flexibility. However, before quantifying EV grid flexibility provision, it is essential to model EV travel patterns and charging behaviors. Traditionally, these models rely on aggregated statistical features of EVs, generated probabilistically, without distinguishing between different EV user types (e.g., retirees, professionals, families with two EVs). This approach lacks the precision needed to accurately quantify flexibility. Therefore, this study employs bottom-up Monte Carlo simulations to achieve high-granularity modeling, enabling a more precise and detailed analysis of travel and charging patterns by categorizing EV users.

3.1. EV user archetypes

According to a UK research report from Project Sciurus, one of the largest V2G demonstration projects in the world, which focuses on the development and deployment of V2G charging technology in the UK [31], the primary residential EV user archetypes can be categorized into three groups. It is worth noting that this study specifically focuses on residential EV users and their grid flexibility provision, excluding other types of EVs such as electric buses or trucks. The three categories of residential EV user archetypes are as follows:

- 1) **One-EV Retiree Household (*Ret-EV*):** This household is occupied by retirees and owns a single EV. *Ret-EV* is equipped with a medium-sized battery and has relatively low annual electricity consumption, reflecting its typical yearly mileage. The EV's time availability, defined as the percentage of hours it is parked and available to connect to the grid throughout the year, is high. The household's trips include shopping and other trips (e.g., for leisure purposes), with no work- or education-related trips.
- 2) **One-EV Professional Household (*Pro-EV*):** This household, occupied by working professionals, also owns a single EV. The *Pro-EV* is equipped with a medium-sized battery but has moderate annual electricity consumption. Its EV time availability is lower than that of the *Ret-EV* (further detailed in Section 6.1). The types of trips taken by this household are more varied, covering a wider range of purposes, which will be detailed in the next subsection.

3) **Two-EV household (Sho-EV and Fam-EV):** This household owns two EVs. The *Sho-EV* is a smaller vehicle primarily used for short trips, such as commuting, equipped with a small battery and moderate annual electricity consumption. Its EV time availability is high, and it is not used for long-distance travel. The *Fam-EV*, a larger vehicle suited for family trips, has a relatively large battery and higher annual electricity consumption. Its time availability is also high, and it is not used for work-related trips such as commuting.

3.2. Travel pattern of different EV user archetypes

Based on data from the UK Department for Transport [32], car travel trips are categorized into four main types:

- 1) Work-related trips (e.g., commuting, business travel);
- 2) Education-related trips (e.g., escorting children to school);
- 3) Shopping trips, made specifically for purchasing goods;
- 4) Other trips (e.g., leisure, personal purposes).

The four types of trips primarily differ in terms of time of occurrence and travel distance. Regarding time of occurrence, work-related trips and education-related trips are assumed not to take place on weekends (any weekend business travel is classified as other trips). These trips typically occur during weekday morning and evening peak hours, aligning with commuting periods for work and school. Their specific departure and arrival times follow certain distributions, which will be discussed in the subsequent paragraphs. In terms of travel distance, based on statistics from the UK Department for Transport [32], the distances for different trip types are assumed to follow a log-normal distribution, with varying mean values. Work-related trips and other trips tend to be longer, averaging 11–13 miles, whereas education-related trips and shopping trips are relatively shorter, with mean distances ranging between 4 and 6 miles.

According to statistical data, EV users typically make between 2 and 5 trips per day (with one trip being a single journey and a round trip counting as 2 trips), averaging about 1000 trips per year. Additionally, based on the characteristics of EV travel, daily trips can be categorized into main trips (which may include adjacent trips) and post-home trips, such as shopping or leisure activities after returning home.

Main trips: These include scenarios with 2 trips (e.g., commuting to

and from work) and 3 trips (e.g., commuting combined with an adjacent trip, such as dropping off children at school before heading to work). Scenarios involving 4 or more trips are relatively rare and complex, and thus excluded from this study. To model the probability of main trips and their adjacent trips, a transition matrix (τ) is used. This 5×4 matrix represents the probability of transitioning from one trip to the next adjacent trip, with the fifth row indicating the probability of starting each of the four trips from home. For each main trip, departure and arrival times at home are determined using a statistical probability distribution (ρ) derived from official data. It is essential to ensure that arrival times occur after departure times, with minimum intervals adjusted according to travel distance. Any generated trip data not meeting these criteria is discarded and regenerated. For adjacent trips, the time intervals between the arrival home time and the departure home time are adjusted based on the distance and type of the adjacent trip.

Post-home trips: These refer to additional round trips made after returning home, usually for activities such as shopping or leisure. These trips typically occur in the afternoon or evening. The final arrival home time for post-home trips is calculated by adding an extra time interval (usually 2 to 3 hours) to the main trip’s arrival home time, depending on the type and distance of the post-home trip.

The distribution of trips for the three EV user archetypes during weekdays and weekends is illustrated in Fig. 3. Notably, the *Ret-EV* maintains a consistent trip pattern across both weekdays and weekends, with neither work-related nor education-related trips. In contrast, the *Pro-EV* may include all four types of trips on weekdays but excludes work-related and education-related trips on weekends. The combination of the *Sho-EV* and *Fam-EV* represents a two-EV household, with each vehicle designated for different types of trips. On weekdays, the *Sho-EV* is primarily used for work-related travel, while the *Fam-EV* is utilized for education-related trips, shopping, and other activities. On weekends, the *Sho-EV* typically remains at home and is not used. The proportions of main trips for each EV user archetype, such as the percentage of families using the *Ret-EV* for shopping or other trips, as well as the proportion of families making post-home trips, are determined using a heuristic method. This approach ensures that the resulting trip counts and proportions, including aggregated charging curves, align with data from the UK Department for Transport [32].

In developing a heuristic method for understanding EV user

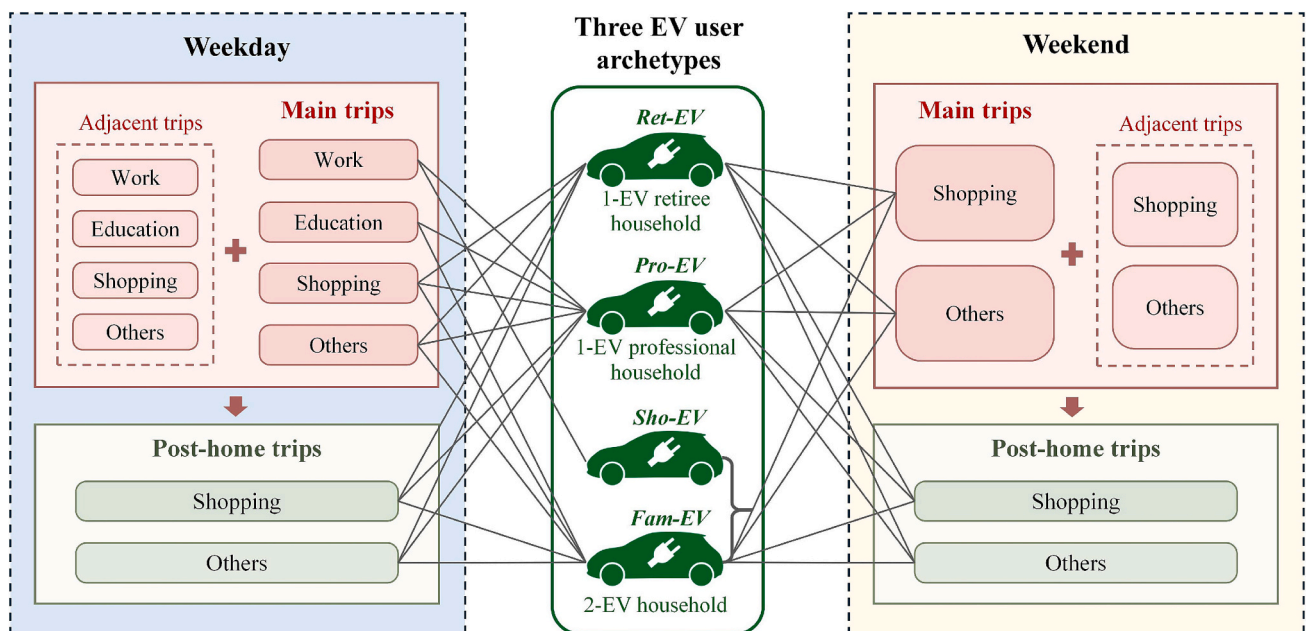


Fig. 3. Associated trips of EV user archetypes on weekdays and weekends.

behavior, several steps are methodically followed: (1) The process begins by estimating the total number of trips annually and weekly based on the annual mileage of each EV user archetype and the average distance per trip, providing foundational data for accurate trip allocation. (2) Trips are allocated between weekdays and weekends, noting specific patterns such as the Ret-EV archetype, which shows no significant difference in trip distribution between weekdays and weekends, and the Sho-EV archetype, which does not take trips on weekends. (3) Key ratios are determined for each archetype, including the distribution of main trips between shopping and other activities, the proportion of adjacent trips, and the proportion of post-home trips. Initial rough estimations of these ratios are conducted based on statistics from the UK Department for Transport. (4) Using the daily trip patterns, travel behavior and corresponding charging patterns are simulated under an immediate charging strategy to model real-world usage and charging scenarios. (5) Finally, the total mileage, departure time distribution, return time distribution, and charging curves are validated against empirical data from the UK Department for Transport. If discrepancies are found, the ratios determined in Step 3 are adjusted in a targeted manner (either increasing or decreasing) to better align with the data, followed by re-simulation. This structured approach guarantees a thorough analysis and accurate validation of EV user behaviors, closely mirroring real-world data, ensuring the reliability and applicability of the findings.

3.3. Charging Patterns

EV users exhibit different charging patterns based on their individual habits and preferences. Generally, they do not always connect their vehicles to a charging point immediately upon arriving home; rather, the decision is primarily influenced by the state of charge (SOC). If the SOC falls below a certain threshold, the EV is plugged in for charging; otherwise, it remains disconnected, leading to zero power injection at those nodes, as reflected in the equation below

$$P_{i,t}^{EVhome} = 0, \quad \forall i \in \Omega_{home}, \quad \text{if } SOC_i^{arr} \geq SOC_i^{threshold} \quad (1)$$

Depending on the frequency of plugging in and the SOC threshold, EV charging patterns—also referred to as charging habits—can be categorized into two types: “graze charge” and “guzzle charge.” In the graze charge pattern, users plug in their EVs frequently, even when the SOC is relatively high. In contrast, the guzzle charge pattern is characterized by less frequent charging, occurring only when the battery is nearly depleted. Naturally, the graze charge pattern results in a higher plug-in rate, increasing the potential for EVs to contribute to grid flexibility.

The frequency of EV users’ participation in V-V2V activities primarily depends on whether they follow a graze charge or guzzle charge pattern. Under graze charge, EV users typically connect to a charging station daily or every two days, allowing them to participate in V-V2V frequently, whereas under guzzle charge, they charge their vehicles only once every one to two weeks. The charging frequency of different EV user archetypes varies due to factors such as battery capacity and daily energy consumption. For instance, *Pro-EV* users tend to have slightly higher travel and charging frequencies compared to *Ret-EV* users, and given the same charging pattern, *Pro-EV* users also connect to the grid and participate in V-V2V more frequently than *Ret-EV* users. However, it is important to note that charging patterns have a significantly greater impact on charging and V-V2V participation frequency than differences in battery capacity or daily energy consumption among users.

4. Modeling V-V2V Incorporating Grid Flexibility Provision

In the previous sections, the concept of V-V2V was defined, along with a high-granularity modeling of EV travel and charging patterns considering categorized EV user archetypes. In this section, the focus shifts to modeling V-V2V grid flexibility provision. This includes a

detailed mathematical model of the V-V2V framework that captures energy sharing among home-charged EVs, as well as between home-charged and public-charged EVs through the low-voltage distribution network. It explains how different EVs share energy within the low-voltage distribution network during charging and discharging. Additionally, the model incorporates a grid flexibility quantification module. EVs can provide multiple forms of grid flexibility through timely charging and discharging, such as backup power and frequency response. However, this paper focuses primarily on the flexibility EVs offer in reducing peak power flows within the grid, including substations and distribution lines. By mitigating peak loads, the model seeks to delay the need for grid expansion, enabling a more efficient and equitable transition using the existing grid infrastructure, without the necessity for costly large-scale upgrades.

4.1. Objective

The objective of the V-V2V model incorporating grid flexibility is to minimize the total energy cost for all users within the low-voltage distribution network, the asset’s present value (APV) cost of grid facilities (e.g., substations and distribution lines), the cost of grid expansion planning, and the degradation cost of EV batteries, whether home-charged or public-charged, as formulated in eqs. (2a)–(2f).

$$\min F = C^{Ener} + C^{Peakflow} + C^{Expan} + C^{V2Ghome} + C^{V2Gpub} \quad (2a)$$

$$C^{Ener} = \sum_t \rho_t^{buy} \cdot P_t^{buy} - \sum_t \rho_t^{sell} \cdot P_t^{sell} \quad (2b)$$

$$C^{Peakflow} = \sum_{ij} (1 - y_{ij}) \cdot APV_{ij} + \sum_{i \in \Omega_{sub}} (1 - y_i) \cdot APV_i \quad (2c)$$

$$C^{Expan} = \frac{1}{365} \sum_{ij} Asset_{ij} \cdot y_{ij} + \frac{1}{365} \sum_{i \in \Omega_{sub}} Asset_i \cdot y_i \quad (2d)$$

$$C^{V2Ghome} = \sum_{i \in \Omega_{home}} \theta^{degra} \frac{\sum_t PD_{i,t}^{EVhome}}{100 \cdot \bar{E}_i^{EVhome}} \cdot Asset_i^{EVhome} \quad (2e)$$

$$C^{V2Gpub} = \sum_{i \in \Omega_{public}} \sum_m \theta^{degra} \frac{\sum_t PD_{i,m,t}^{EVpub}}{100 \cdot \bar{E}_{i,o(m)}^{EVpub}} \cdot Asset_{i,o(m)}^{EVpub} \quad (2f)$$

Specifically, eq. (2b) represents the total energy cost for all users, which is the cost of energy purchased from the utility company minus the revenue from energy sold back to the utility company. In the V-V2V framework, users share energy through the low-voltage distribution network, with any energy deficit being purchased from the utility company, while surplus energy is sold back. Eq. (2c) accounts for the sum of APVs of substations and distribution lines. For each grid facility, its APV is modeled as a piecewise linear function that varies with headroom. As peak power flow on the grid increases, the headroom rate (i.e., the ratio of the remaining capacity of a grid facility to its total capacity) decreases, signaling a greater need for future investment (i.e., earlier expansion planning). As a result, the present value of the asset’s investment cost rises. The detailed relationship between APV and the headroom rate is discussed in subsection 4.5.

Eq. (2d) represents the sum of daily investment costs for grid facilities. It is important to note that APV and investment costs are treated as mutually exclusive in this study. If a grid facility requires immediate expansion due to insufficient capacity, only the investment costs are considered. Conversely, if there is remaining capacity (i.e., headroom rate is greater than 0), only the APV is taken into account. This is why both y_{ij} and y_i binary variables are included in eqs. (2c) and (2d) to reflect this non-additive relationship. Eqs. (2e) and (2f) represent the degradation costs of home-charged EV and public-charged EV batteries, respectively. In these equations, θ^{degra} denotes the percentage of battery

capacity degradation per complete charge-discharge cycle, while $\sum_t PD_{i,t}^{EVhome} / \bar{E}_i^{EVhome}$ represents the proportion of discharge energy relative to the EV battery's capacity over the simulation period. Since the discharged energy is recharged during the corresponding period, this proportion can be interpreted as the charge-discharge cycle proportion coefficient. In these equations, i denotes the index of the node, and ij represents the index of the lines connecting nodes i and j .

The objective function and its components described in (2a)–(2f) are based on the V-V2V framework. In the non-V-V2V framework, where each EV user independently determines their charging and discharging behavior primarily based on time-of-use pricing, the objective function is structured as shown in eqs. (3a)–(3c).

$$\min F = C^{Ener} + C^{Expn} + C^{V2Ghome} + C^{V2Gpub} \quad (3a)$$

$$C^{Ener} = \sum_{i,t} \rho_t^{buy} \cdot P_{i,t}^{in} - \sum_{i,t} \rho_t^{sell} \cdot P_{i,t}^{out} \quad (3b)$$

$$(2d) - (2f) \quad (3c)$$

First, regarding the total energy cost, since each user independently interacts with the utility company without V-V2V energy sharing, the total energy cost is represented by eq. (3b), differing from (2b). Additionally, because individual users cannot directly perceive or influence the peak flow of grid facilities through their charging and discharging actions, the objective function does not include the costs related to the APV of grid facilities, which are affected by peak flow and headroom rate. However, the cost components described in eqs. (2d)–(2f) are still applicable in the non-V-V2V framework, as reflected in eq. (3c). This is because EV charging and discharging must still adhere to the constraints of the low-voltage distribution network. If capacity limits are exceeded, grid facility expansion planning remains necessary. Moreover, EV battery degradation costs continue to apply as long as EVs engage in V2G operations.

4.2. Distribution network constraints

In this study, a simplified AC power flow model for distribution networks is adopted [33]. This model accounts for voltage drops caused by impedance when transmitting active and reactive power. To enable rapid computation across large-scale networks and various scenarios, network losses are ignored. However, it is worth noting that the model can be extended to include network losses. This could be achieved by either assuming a relatively fixed loss coefficient or by expanding the current model into a classic second-order cone optimization problem that incorporates network loss constraints in radial distribution networks [34].

$$\sum_{j \in ST(i)} PL_{ij,t} = P_{i,t}^{sub}, \quad \sum_{j \in ST(i)} QL_{ij,t} = Q_{i,t}^{sub}, \quad \forall i \in \Omega_{sub}, \quad \forall t \quad (4)$$

$$\sum_{j \in ED(i)} PL_{ji,t} - \sum_{j \in ST(i)} PL_{ij,t} + PV_{i,t} = PD_{i,t}^{nonEV} + P_{i,t}^{EVhome}, \quad \forall i \in \Omega_{home}, \quad \forall t \quad (5)$$

$$\sum_{j \in ED(i)} PL_{ji,t} - \sum_{j \in ST(i)} PL_{ij,t} + PV_{i,t} = PD_{i,t}^{nonEV} + \sum_m P_{i,m,t}^{EVpub}, \quad \forall i \in \Omega_{public}, \quad \forall t \quad (6)$$

$$\sum_{j \in ED(i)} QL_{ji,t} - \sum_{j \in ST(i)} QL_{ij,t} = QD_{i,t}^{nonEV}, \quad \forall i \in \Omega_{public} \cup \Omega_{home}, \quad \forall t \quad (7)$$

$$P_{i,t}^{in} - P_{i,t}^{out} = PD_{i,t}^{nonEV} - PV_{i,t} + P_{i,t}^{EVhome}, \quad \forall i \in \Omega_{home}, \quad \forall t \quad (8)$$

$$P_{i,t}^{in} - P_{i,t}^{out} = PD_{i,t}^{nonEV} - PV_{i,t} + \sum_m P_{i,m,t}^{EVpub}, \quad \forall i \in \Omega_{public}, \quad \forall t \quad (9)$$

$$\sum_i (P_{i,t}^{in} - P_{i,t}^{out}) = P_t^{buy} - P_t^{sell}, \quad \forall t \quad (10)$$

$$P_{i,t}^{in}, P_{i,t}^{out}, P_t^{buy}, P_t^{sell} \geq 0, \quad \forall i, \forall t \quad (11)$$

Firstly, constraints (4)–(11) introduce the nodal power balance constraints, along with the representation of nodal power injection or output and the hourly power purchase or selling. Specifically, constraint (4) enforces the active and reactive power balance at nodes with substations, ensuring that the power from the substation equals the sum of the power flowing through the downstream lines connected to that node. Constraints (5) and (6) represent the active power balance for nodes with home-charged EVs and public parking lots, respectively. On the left side of these equations is the net active power inflow (i.e., the active power injected from upstream lines minus the power flowing to downstream lines) plus PV generation, while the right side represents the total load at the node, which is the sum of non-EV and EV loads. Similarly, constraint (7) ensures the reactive power balance for these two types of nodes. Additionally, constraints (8) and (9) define the formulaic expressions for active power injection or power output at nodes with home-charged EVs and public parking lots, respectively. The relationship between active power injection or output at each node and the power purchase or sale by all users to the utility company is governed by constraint (10). Finally, constraint (11) ensures the non-negativity of active power injection, power output, and electricity transactions with the utility company.

$$0 \leq PV_{i,t} \leq \bar{PV}_{i,t}, \quad \forall i, \forall t \quad (12)$$

$$U_{i,t} - U_{j,t} = PL_{ij,t} \cdot R_{ij} + QL_{ij,t} \cdot X_{ij}, \quad \forall ij, \forall t \quad (13)$$

$$\underline{U} \leq U_{i,t} \leq \bar{U}, \quad \forall i, \forall t \quad (14)$$

$$\sqrt{PL_{ij,t}^2 + QL_{ij,t}^2} \leq \bar{S}_{ij} \cdot (1 + y_{ij}), \quad \forall ij, \forall t \quad (15)$$

$$\sqrt{(P_{i,t}^{sub})^2 + (Q_{i,t}^{sub})^2} \leq \bar{S}_i \cdot (1 + y_i), \quad \forall i \in \Omega_{sub}, \forall t \quad (16)$$

$$\sqrt{PL_{ij,t}^2 + QL_{ij,t}^2} \leq S_{ij}^{Peakflow} + \bar{S}_{ij} \cdot y_{ij}, \quad \forall ij, \forall t \quad (17)$$

$$HR_{ij} = (\bar{S}_{ij} - S_{ij}^{Peakflow}) / \bar{S}_{ij}, \quad \forall ij \quad (18)$$

$$\sqrt{(P_{i,t}^{sub})^2 + (Q_{i,t}^{sub})^2} \leq S_i^{Peakflow} + \bar{S}_i \cdot y_i, \quad \forall i \in \Omega_{sub}, \forall t \quad (19)$$

$$HR_i = (\bar{S}_i - S_i^{Peakflow}) / \bar{S}_i, \quad \forall i \in \Omega_{sub} \quad (20)$$

Then, constraints (12)–(20) cover the security constraints, which include the power limits of PV systems, the voltage limits, and the capacity limits of power lines and substations. Constraint (12) sets the upper and lower limits for PV generation. Constraints (13) and (14) are voltage constraints: constraint (13) defines the relationship between voltage drop across each line, power flow, and line impedance, while constraint (14) provides the upper and lower voltage limits. Constraints (15) and (16) impose capacity limits for each line and substation, respectively. Constraints (17) and (18) establish the relationship between the line headroom rate and its peak flow, where the peak flow is defined as the maximum apparent power of the line during the simulation period, as described in (17). Similarly, constraints (19) and (20) define the relationship between the substation headroom rate and its peak flow, with the peak flow representing the maximum apparent power of the substation during the simulation period, as shown in (19).

4.3. Home-charged EVs operational constraints

In this section, the operational constraints for home-charged EVs are defined. As previously mentioned, it is assumed that every node without

a substation or public parking lot is a node with home-charged EVs. However, in reality, not every household owns an EV. Therefore, nodes with home-charged EVs may also include users without EVs, where the EV battery capacity is effectively zero. It is important to note that while the majority of EV charging in the UK typically occurs at home, and this study primarily focuses on EV charging within residential communities, the use of public charging facilities outside of these communities (e.g., at workplaces) is also accounted for in the analysis. This external charging is mainly reflected in the calculation of the arrive-home SOC SOC_i^{arr} . When EVs leave home for long trips or start with a low depart-home SOC, the remaining battery SOC after the departure trip may not suffice for completing the return journey. In such instances, it is assumed that the EVs will charge at locations outside of the home. The arrive-home SOC is then updated based on the EV's remaining trips for the day.

To account for this, constraint (21) is introduced to represent users without EVs, ensuring that the EV power injection at these nodes is zero.

$$P_{i,t}^{EVhome} = 0, \quad \forall i \in \Omega_{home}, \quad \text{if } \bar{E}_i^{EVhome} = 0 \quad (21)$$

Additionally, it is important to note that some households have one EV, while others have two. For households with two EVs, it is assumed that both vehicles share a single charging point. Given the typical driving range of EVs, which often allows for more than ten days of usage before the battery is fully depleted, it is feasible for two EVs to alternate their charging schedules at a shared private charging point. In this study, it is assumed that within a 24-h simulation period, only one of the two EVs will be connected to the home charging point at any given time, following a first-come, first-served principle based on the SOC of each EV.

$$P_{i,t}^{EVhome} = PC_{i,t}^{EVhome} - PD_{i,t}^{EVhome}, \quad \forall i \in \Omega_{home}, \quad \forall t \quad (22)$$

$$0 \leq PC_{i,t}^{EVhome} \leq \bar{P}_i^{Homecharger}, \quad \forall i \in \Omega_{home}, \quad \forall t \quad (23)$$

$$0 \leq PD_{i,t}^{EVhome} \leq \bar{P}_i^{Homecharger}, \quad \forall i \in \Omega_{home}, \quad \forall t \quad (24)$$

$$0 \leq E_{i,t}^{EVhome} \leq \bar{E}_i^{EVhome}, \quad \forall i \in \Omega_{home}, \quad \forall t \quad (25)$$

$$E_{i,t}^{EVhome} = SOC_i^{arr} / 100 \cdot \bar{E}_i^{EVhome}, \quad \forall i \in \Omega_{home}, \quad \forall t = t_i^{arr} \quad (26)$$

$$E_{i,t}^{EVhome} = SOC_i^{Nextdep} / 100 \cdot \bar{E}_i^{EVhome}, \quad \forall i \in \Omega_{home}, \quad \forall t = t_i^{Nextdep} \quad (27)$$

In addition to the constraints in (21), constraint (1) is incorporated to account for charging patterns, while constraints (22) through (27) represent standard operational constraints governing battery storage charging and discharging. Constraint (22) defines the power injection of home-charged EVs, accounting for their charging and discharging power. Constraints (23) and (24) establish the bounds for charging and discharging power, ensuring that it is non-negative and does not exceed the maximum charging power (i.e., the rated power of the charger). Constraint (25) limits the stored energy of home-charged EV batteries to remain between zero and the battery's rated capacity. Constraint (26) assigns values to the time periods when home-charged EVs are connected to the charging point (i.e., upon arriving home) and their corresponding SOC. Constraint (27) specifies the time periods when home-charged EVs disconnect from the charging point (i.e., the next time they depart from home) and their SOCs.

It should be noted that an EV may arrive and depart from home multiple times within a single day, resulting in several non-continuous periods when it is connected to the grid. However, this study focuses only on the primary connection hours, typically from the evening arrival after work to the next morning's departure. This assumption is reasonable given current EV user plug-in behaviors, as most owners do not plug in their EVs every time they return home. Under this assumption, there are two possible scenarios for the arrival (t_i^{arr}) and next departure

($t_i^{Nextdep}$) times. The first scenario is when the EV arrives in the evening and departs the next day during daylight hours, which is quite common. The second scenario occurs when the EV arrives home in the early morning (e.g., 1 a.m.) and departs later that same day. In both cases, the difference in stored energy between adjacent time periods, as well as the corresponding charging and discharging relationships, are captured by constraints (28) and (29), respectively.

$$\forall i \in \Omega_{other}, \quad \text{if } t_i^{arr} \text{ and } t_i^{Nextdep} \text{ are not on the same day}$$

$$\begin{cases} E_{i,t+1}^{EVhome} = E_{i,t}^{EVhome} + PC_{i,t}^{EVhome} \cdot \eta - PD_{i,t}^{EVhome} / \eta, \quad \forall t = t_i^{arr} \dots 23 \\ E_{i,t+1}^{EVhome} = E_{i,t}^{EVhome} + PC_{i,t}^{EVhome} \cdot \eta - PD_{i,t}^{EVhome} / \eta, \quad \forall t = 1 \dots t_i^{Nextdep} - 1 \\ E_{i,1}^{EVhome} = E_{i,24}^{EVhome} + PC_{i,24}^{EVhome} \cdot \eta - PD_{i,24}^{EVhome} / \eta \\ P_{i,t}^{EVhome} = 0, \quad \forall t = t_i^{Nextdep} \dots t_i^{arr} - 1 \end{cases} \quad (28)$$

$$\forall i \in \Omega_{other}, \quad \text{if } t_i^{arr} \text{ and } t_i^{Nextdep} \text{ are on the same day}$$

$$\begin{cases} E_{i,t+1}^{EVhome} = E_{i,t}^{EVhome} + PC_{i,t}^{EVhome} \cdot \eta - PD_{i,t}^{EVhome} / \eta, \quad \forall t = t_i^{arr} \dots t_i^{Nextdep} - 1 \\ P_{i,t}^{EVhome} = 0, \quad \forall t \neq t_i^{arr} \dots t_i^{Nextdep} - 1 \end{cases} \quad (29)$$

Specifically, the first three mathematical expressions in constraint (28) define the relationship between the change in stored energy across adjacent time periods and the charging or discharging power during those periods (considering charging and discharging efficiency). This relationship applies from the EV's arrival time on the previous day to its departure time the following day. The fourth expression indicates that during other periods, when the EV is not connected to the grid, there is zero power injection, meaning no charging or discharging power. Similarly, the first mathematical expression in constraint (29) defines the relationship between the change in stored energy across adjacent time periods and the charging or discharging power during those periods, from the EV's arrival time to its departure time on the same day. The second expression shows that during other periods, when the EV is not connected to the grid, the power injection is zero.

4.4. Public-charged EVs operational constraints

In the previous subsection, the operational constraints for home-charged EVs were introduced. This section focuses on the operational constraints for public-charged EVs. Unlike home-charged EVs, which charge only when the SOC falls below a threshold, public-charged EVs do not have dedicated charging points and must share limited charging stations in public parking lots with other vehicles. As a result, the number of public-charged EVs exceeds the available charging points, leading to "charging anxiety." Due to this charging anxiety, the plugging and charging strategy for public-charged EVs differs from that of home-charged EVs. First, public-charged EVs with an SOC below the threshold upon arrival are given the highest charging priority, assuming they have secured a charging point in advance through a reservation system. For public-charged EVs with an SOC above the threshold, charging anxiety persists due to the uncertainty of securing a charging point in the following days. Therefore, if there are unoccupied charging points upon their arrival and their SOC is not excessively high, they will attempt to secure a charging point and begin charging. In such cases, the first-come, first-served principle applies until all charging points are occupied. Based on these settings and assumptions, the operational constraints for public-charged EVs are formulated in constraints (30)–(37).

$$P_{i,m,t}^{EVpub} = PC_{i,m,t}^{EVpub} - PD_{i,m,t}^{EVpub}, \quad \forall i \in \Omega_{public}, \quad \forall m, \quad \forall t \quad (30)$$

$$0 \leq PC_{i,m,t}^{EVpub} \leq \bar{P}_{i,m}^{Publiccharger}, \quad \forall i \in \Omega_{public}, \quad \forall m, \quad \forall t \quad (31)$$

$$0 \leq PD_{i,o(m),t}^{EVpub} \leq \bar{P}_{i,m}^{Pubcharger}, \quad \forall i \in \Omega_{public}, \forall m, \forall t \quad (32)$$

$$0 \leq E_{i,o(m),t}^{EVpub} \leq \bar{E}_{i,o(m)}^{EVpub}, \quad \forall i \in \Omega_{public}, \forall m, \forall t \quad (33)$$

$$E_{i,o(m),t}^{EVhome} = SOC_{i,o(m)}^{arr} / 100 \cdot \bar{E}_{i,o(m)}^{EVhome}, \quad \forall i \in \Omega_{public}, \forall m, \forall t = t_{i,o(m)}^{arr} \quad (34)$$

$$E_{i,o(m),t}^{EVhome} = SOC_{i,o(m)}^{Nextdep} / 100 \cdot \bar{E}_{i,o(m)}^{EVhome}, \quad \forall i \in \Omega_{public}, \forall m, \forall t = t_{i,o(m)}^{Nextdep} \quad (35)$$

Specifically, constraint (30) defines the power injection for each charging point in the public parking lot, relating it to the charging and discharging power. Constraints (31) and (32) establish charging and discharging power limits, ensuring it remains non-negative and does not exceed the maximum charging capacity. Constraint (33) restricts the stored energy of public-charged EV batteries to between zero and their rated capacity. Constraint (34) assigns values to the arrival times of public-charged EVs and their corresponding SOC, while constraint (35) assigns values to their next departure times and SOC.

$$\forall i \in \Omega_{public}, \text{ if } t_{i,o(m)}^{arr} \text{ and } t_{i,o(m)}^{Nextdep} \text{ are on the same day}$$

$$\begin{cases} E_{i,o(m),t+1}^{EVhome} = E_{i,o(m),t}^{EVhome} + PC_{i,m,t}^{EVhome} \cdot \eta - PD_{i,m,t}^{EVhome} / \eta, \quad \forall t = t_{i,o(m)}^{arr} \dots 23 \\ E_{i,o(m),t+1}^{EVhome} = E_{i,o(m),t}^{EVhome} + PC_{i,m,t}^{EVhome} \cdot \eta - PD_{i,m,t}^{EVhome} / \eta, \quad \forall t = 1 \dots t_{i,o(m)}^{Nextdep} - 1 \\ E_{i,o(m),1}^{EVhome} = E_{i,o(m),24}^{EVhome} + PC_{i,m,24}^{EVhome} \cdot \eta - PD_{i,m,24}^{EVhome} / \eta \\ P_{i,m,t}^{EVhome} = 0, \quad \forall t = t_{i,o(m)}^{Nextdep} \dots t_{i,o(m)}^{arr} - 1 \end{cases} \quad (36)$$

$$\forall i \in \Omega_{public}, \text{ if } t_{i,o(m)}^{arr} \text{ and } t_{i,o(m)}^{Nextdep} \text{ are on the same day}$$

$$\begin{cases} E_{i,o(m),t+1}^{EVhome} = E_{i,o(m),t}^{EVhome} + PC_{i,m,t}^{EVhome} \cdot \eta - PD_{i,m,t}^{EVhome} / \eta, \quad \forall t = t_{i,o(m)}^{arr} \dots t_{i,o(m)}^{Nextdep} - 1 \\ P_{i,m,t}^{EVhome} = 0, \quad \forall t \neq t_{i,o(m)}^{arr} \dots t_{i,o(m)}^{Nextdep} - 1 \end{cases} \quad (37)$$

Similar to home-charged EVs, this study only considers the continuous primary connection hours with the grid during the 24-h simulation period, typically from evening arrival after work to the next morning's departure. There are two possible scenarios for the arrival and next departure times. The first is when they occur on different days, such as when the EV arrives in the evening and departs the following day during daylight hours. The second scenario occurs when the EV arrives in the early morning and departs later the same day. The first case is modeled in constraint (36), where the first three mathematical expressions define the relationship between the change in stored energy across adjacent time periods and the corresponding charging and discharging power. This relationship applies from the EV's arrival on the previous day to its departure the next day. The fourth expression indicates that during other periods, when the EV is not connected to the grid, there is zero power injection. The second case is captured in constraint (37), where the first mathematical expression establishes the relationship between the change in stored energy across adjacent time periods and the charging and discharging power for the span from the EV's arrival to its departure on the same day. The second expression specifies that during other periods, the EV is not connected to the grid, resulting in zero power injection.

4.5. Operational constraints for quantifying grid flexibility provision

In this subsection, operational constraints for quantifying grid flexibility provision are detailed. The primary focus of this paper's V-V2V grid flexibility quantification is to assess the contribution of V-V2V in reducing the peak flow of grid facilities, thereby increasing the headroom rate. Specifically, the relationship between the headroom rate of grid facilities and the APV is established. By incorporating and

minimizing the APV in the V-V2V framework's objective function, the headroom rate can be effectively enhanced. The relationship between APV and headroom rate (HR) is presented in eq. (38a).

$$APV = \frac{Asset}{(1 + DR)^{-\log(1-HR)/\log(1+LGR)}} \quad (38a)$$

The derivation of expression (38a) is detailed through eqs. (38b) to (38e). Specifically, assume the grid facility's capacity is \bar{S} , and its current peak flow is $S^{Peakflow}$. Given a relatively fixed annual load growth rate LGR , it means that in n^{year} years, the grid facility's capacity will be exhausted, as shown in (38b). Considering the relationship between HR and $S^{Peakflow}$ as shown in eq. (38c), the derived relationship between n^{year} and HR can be expressed in eq. (38d). Additionally, the net present value of the APV is given by expression (38e) as a function of the asset value, discount rate (DR), and n^{year} . By substituting (38d) into (38e), the final expression shown in (38a) is obtained.

$$\bar{S} = S^{Peakflow} (1 + LGR)^{n^{year}} \quad (38b)$$

$$HR = 1 - S^{Peakflow} / \bar{S} \quad (38c)$$

$$n^{year} = -\log(1 - HR) / \log(1 + LGR) \quad (38d)$$

$$APV = Asset / (1 + DR)^{n^{year}} \quad (38e)$$

Constraint (38a) is a highly nonlinear equation that can be reformulated into a piecewise linear form. Eqs. (39a)-(39c) describe the piecewise linear relationship between the APV and the headroom rate for each line. Specifically, (39a) indicates that the headroom rate for each line is divided into K segments, and the APV is the initial value of the function (i.e., the asset value) plus the incremental function value for each segment (i.e., the slope of the piecewise linear function, which is a negative value, multiplied by the k -th segmental headroom rate), as shown in (39b). The upper and lower bounds of the segmental headroom rate are constrained by (39c).

$$HR_{ij} = \sum_{k=1}^K \Delta HR_{ij,k}, \quad \forall ij \quad (39a)$$

$$APV_{ij} = Asset_{ij} + \sum_{k=1}^K Slope_{ij,k} \cdot \Delta HR_{ij,k}, \quad \forall ij \quad (39b)$$

$$0 \leq \Delta HR_{ij,k} \leq \overline{\Delta HR}_{ij}, \quad \forall ij, \forall k \quad (39c)$$

Similarly, eqs. (40a)-(40c) describe the piecewise linear relationship between the APV and the headroom rate for substations. The interpretation of these constraints is entirely analogous to the corresponding constraints in eqs. (39a)-(39c).

$$HR_i = \sum_{k=1}^K \Delta HR_{i,k}, \quad \forall i \in \Omega_{sub} \quad (40a)$$

$$APV_i = Asset_i + \sum_{k=1}^K Slope_{i,k} \cdot \Delta HR_{i,k}, \quad \forall i \in \Omega_{sub} \quad (40b)$$

$$0 \leq \Delta HR_{i,k} \leq \overline{\Delta HR}_i, \quad \forall i \in \Omega_{sub}, \forall k \quad (40c)$$

5. Statistically Similar Network-Based Method for Quantifying Grid Flexibility

While Section 4 develops a mathematical model to assess V-V2V incorporating grid flexibility provision, that model is based on a single power distribution network, and applying it alone limits its broader statistical generalisability. To address this, Section 5 introduces the statistically similar network-based method, which extends the analysis by evaluating V-V2V's impact across a series of statistically similar

networks defined by topological and electrical parameters rather than relying on just one. By incorporating multiple statistically similar networks, Section 5 enhances its robustness and applicability compared to relying solely on the model from Section 4, ensuring that the results can be more confidently extended to real-world power distribution systems.

Specifically, the proposed statistically similar networks method enhances the assessment of V-V2V grid flexibility by addressing both substation-level and internal line-level impacts. At the substation level, it provides more robust, credible, and universally applicable results by incorporating statistical diversity across multiple networks rather than considering variations in distributed energy resources (DERs) alone. Beyond substation-level flexibility provision, the method further accounts for internal line congestion, a critical issue in low-voltage distribution networks with large-scale EV integration. By considering the statistical characteristics of peak flow and headroom at the internal line level, it enables a more granular analysis of how V-V2V improves network capacity utilization and reduces congestion. Overall, by generating a set of networks that share similar topological and electrical characteristics, this approach allows for quantitative analyses that are both diverse and comparable, ensuring statistically meaningful insights at both substation and internal line levels. The following subsections will detail the methodology for generating statistically similar networks and the associated quantification process.

5.1. Network division and key topological and electrical parameter identification

The generation of statistically similar networks in this study is based on identifying key topological and electrical features from the input networks and establishing probability distributions for these features, whether discrete (e.g., the total number of nodes, line types, capacities, and impedances) or continuous (e.g., the length of each line). The topological parameters include basic network information such as the total number of nodes, as well as key features that provide a comprehensive understanding of the network's structure. These features include the node degree, which indicates the connectivity of a particular node by counting its direct connections (lines), and the node height, defined as the length of the longest path from the node to any of its leaf nodes (terminal nodes with no further branches). As shown in Fig. 4, each node's degree and height values are provided. Based on node height within the radial distribution network, the network is divided into three levels: near-substation, intermediate, and near-terminal user levels. For example, in Fig. 4, six nodes with a height of 0 belong to the near-

terminal user level, nine nodes with heights of 1 or 2 fall into the intermediate level, and six nodes with heights between 3 and 5 are classified in the near-substation level. This classification ensures a balanced distribution of nodes across levels, with the 21 non-substation nodes distributed among the three levels, ranging from 6 to 9 nodes per level, averaging approximately 7 nodes per level.

Once the levels are defined, discrete probability distribution functions for node degree and height are calculated for nodes within each level, alongside continuous probability distribution functions for line lengths within those levels. Additionally, key topological features such as the number of leaf nodes, the total number of nodes, the number of nodes per level, and the overall network height (substation node height) are identified. In terms of electrical features, this includes generating probability distribution functions for the capacity or peak values of substations and loads, as well as the types of lines, which determine their rated capacity and unit length impedance. After dividing the network into near-substation, intermediate, and near-terminal levels, and obtaining probability statistics for key topological and electrical characteristics at each level and across the entire network, the process of generating the network can begin.

5.2. Network topology and electrical parameters generation

The generation process begins with the leaf nodes. Nodes directly connected to the leaf nodes are then generated and assigned node degree and node height values based on the pre-generated probability distribution functions for the near-terminal user level. Line length values are also assigned according to their probability distribution functions. Once the number of nodes in this level falls within its predefined range, the network generation process proceeds to the next level. Similarly, nodes and lines are generated according to the corresponding probability distribution functions. After the nodes and lines in the near-substation level are completed, the network topology and topological parameters are generated. A check is conducted to ensure that the overall topology—such as network height and total number of nodes—is comparable to the input networks. If the check is successfully passed, the process moves forward to generating the electrical parameters. Otherwise, the network topology is discarded, and the generation process is repeated.

For electrical parameter generation, the capacity or peak values of substations and loads, as well as the types of lines determining the rated capacity and unit length impedance in each level, are assigned via their probability distribution functions. Once all electrical parameters for the

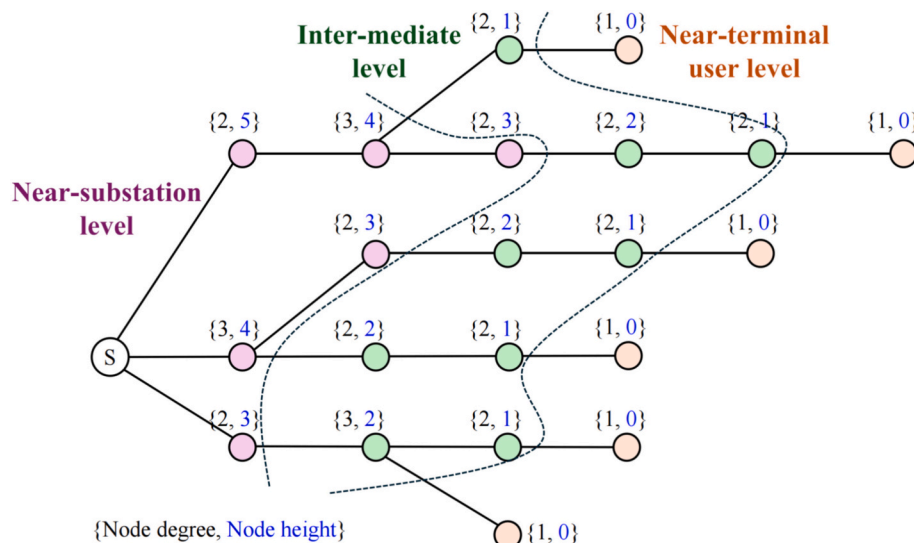


Fig. 4. Illustration of an exemplified low-voltage distribution network.

loads, lines, and substation are assigned, a check is performed. Specifically, a power flow calculation is conducted to ensure that the assigned electrical parameters for the current network topology do not cause any thermal capacity or voltage violations. If the check fails, the network is discarded, and the generation process is repeated for both topological and electrical parameters. If the check is successfully passed, the topological and electrical parameters are considered matched and reasonable.

5.3. Graph theory-based network similarity validation

It's important to note that even though the topological and electrical parameters are considered matched and reasonable, and both sets of parameters are generated from the probability distribution functions identified from the input networks, there is no guarantee that the generated networks are truly similar to the input networks. This is primarily due to the lack of consideration for the correlation between topological and electrical parameters. Specifically, while the topology of the generated network may resemble the input network, and the electrical characteristics may also be similar, the overall similarity could be weak if the correlation between these parameters is not preserved. Therefore, it is necessary to verify whether the generated network is similar to the input network by considering the correlation between topological and electrical parameters. This study proposes a graph theory-based network similarity validation to ensure that the generated networks are similar to the input networks, not only in individual topological and electrical parameters but also in the correlation between these two categories.

Specifically, the matrix representation of the graph is introduced using an adjacency matrix to depict the network topology. This matrix shows the connections between nodes, where traditionally a value of 1 indicates the presence of a line between nodes. To enhance this representation, the value of 1 is replaced with values that reflect line impedance, thereby capturing more detailed electrical characteristics. Additionally, to represent the electrical properties of the nodes, the load values are placed on the diagonal of the matrix. This results in a modified node-node adjacency matrix. The similarity between the generated network and the input network is then evaluated using this modified adjacency matrix. Three metrics are employed for this evaluation: cosine similarity, spectral similarity using the Laplacian matrix, and graph edit distance. Together, these metrics provide a comprehensive assessment of the correlation between the generated and input networks.

Cosine similarity is a measure of similarity between two non-zero vectors in an inner product space. It is calculated as the cosine of the angle between the two vectors, which is also the dot product of the vectors divided by the product of their magnitudes. In the context of graph adjacency matrices, the matrices can be flattened into vectors, and cosine similarity can then be used to measure the similarity between these vectors. To calculate the cosine similarity between two matrices A_g and A_i from the generated network and the input network, respectively, first flatten the matrices into vectors $\text{vec}(A_g)$ and $\text{vec}(A_i)$. The formula for cosine similarity is:

$$\text{cosine_similarity}(\text{vec}(A_g), \text{vec}(A_i)) = \frac{\text{vec}(A_g) \cdot \text{vec}(A_i)}{\|\text{vec}(A_g)\| \|\text{vec}(A_i)\|} \quad (41)$$

The Laplacian matrix L of a graph is defined as $L = D - A$, where D is the degree matrix (a diagonal matrix where each element D_{ii} is the degree of node i), and A is the revised adjacency matrix. Spectral similarity involves comparing the eigenvalues (or spectrum) of the Laplacian matrices of the generated and input networks. Similar eigenvalues suggest similar structural properties of the networks. To compare spectral similarity, the eigenvalues of the Laplacian matrices of both the generated network L_g and the input network L_i are computed. Let $\lambda_{g,k}$ and $\lambda_{i,k}$ be the sorted eigenvalue vectors of L_g and L_i , respectively. The spectral similarity can then be quantified by measuring the distance

between these eigenvalue vectors:

$$\text{spectral_similarity}(L_g, L_i) = \sqrt{\sum_k (\lambda_{g,k} - \lambda_{i,k})^2} \quad (42)$$

where $\lambda_{g,k}$ and $\lambda_{i,k}$ are the k -th eigenvalues of the generated and input networks' Laplacian matrices, respectively.

Graph Edit Distance (GED) is a measure of similarity between two graphs, quantifying the minimum number of operations needed to transform one graph into the other, including node and edge insertions, deletions, and substitutions. As shown in formula (43), GED combines two key components: Edge Edit Distance, which measures the sum of absolute differences in the edge weights between the adjacency matrices of the two graphs, normalized to account for symmetry; and Node Edit Distance, which accounts for the differences in nodal parameters represented by the diagonal elements of the adjacency matrices. By summing these components, GED provides a comprehensive metric that captures both the topological and electrical differences between the two graphs.

$$\text{GED}(L_g, L_i) = \frac{1}{2} \sum_{m=1}^N \sum_{n=1}^N |L_{g,mn} - L_{i,mn}| + \sum_{n=1}^N |\text{diag}(L_g)_n - \text{diag}(L_i)_n| \quad (43)$$

5.4. Quantification process of V-V2V's grid flexibility provision using statistically similar networks

The flowchart presented in Fig. 5 outlines the quantification process of V-V2V's grid flexibility provision using statistically similar networks.

It begins with the division of the network, followed by identifying key topological and electrical parameters. These parameters are then statistically analyzed, and their probability density functions are calculated. Afterward, the process generates new network topologies, which are compared against the input network to check for similarity. If the topologies are sufficiently similar, electrical parameters are generated for the new network. These electrical parameters are then validated, and only networks that pass the validation proceed. The next step involves a graph-theory-based similarity measurement between the input and generated networks. If the generated network passes the graph-theory validation, it is used for quantifying grid flexibility, specifically for V2V flexibility provision. If any step in this process fails, the network is discarded, and the process repeats with a new topology. This ensures the generation of statistically robust and valid networks.

6. Case Studies

6.1. Cases and system descriptions

To validate the effectiveness of the proposed V-V2V framework, four EV charging modes and corresponding cases are designed for comparison: 1) Immediate Charge: Once the EV is connected to the distribution network, it begins charging at maximum power until it reaches the target battery SOC; 2) Smart Charge: Only unidirectional charging is allowed, and while discharging to the grid is prohibited, EVs can adjust their charging times based on time-of-use pricing; 3) V2G: Bidirectional charging and discharging are allowed, and EVs can optimize their charging and discharging power and times according to time-of-use electricity prices to minimize electricity costs; 4) V-V2V: Bidirectional charging and discharging are allowed, and energy sharing is permitted between both home-charged and public-charged EVs connected to the same distribution network. Accordingly, EV charging and discharging decisions are based not only on electricity prices but also on mitigating network capacity pressures—reducing peak loads on facilities such as substations and power lines. Additionally, the statistically similar network method is applied using a British low-voltage distribution network (shown in Fig. 6) as the input network.

A set of networks are then generated that are statistically similar in

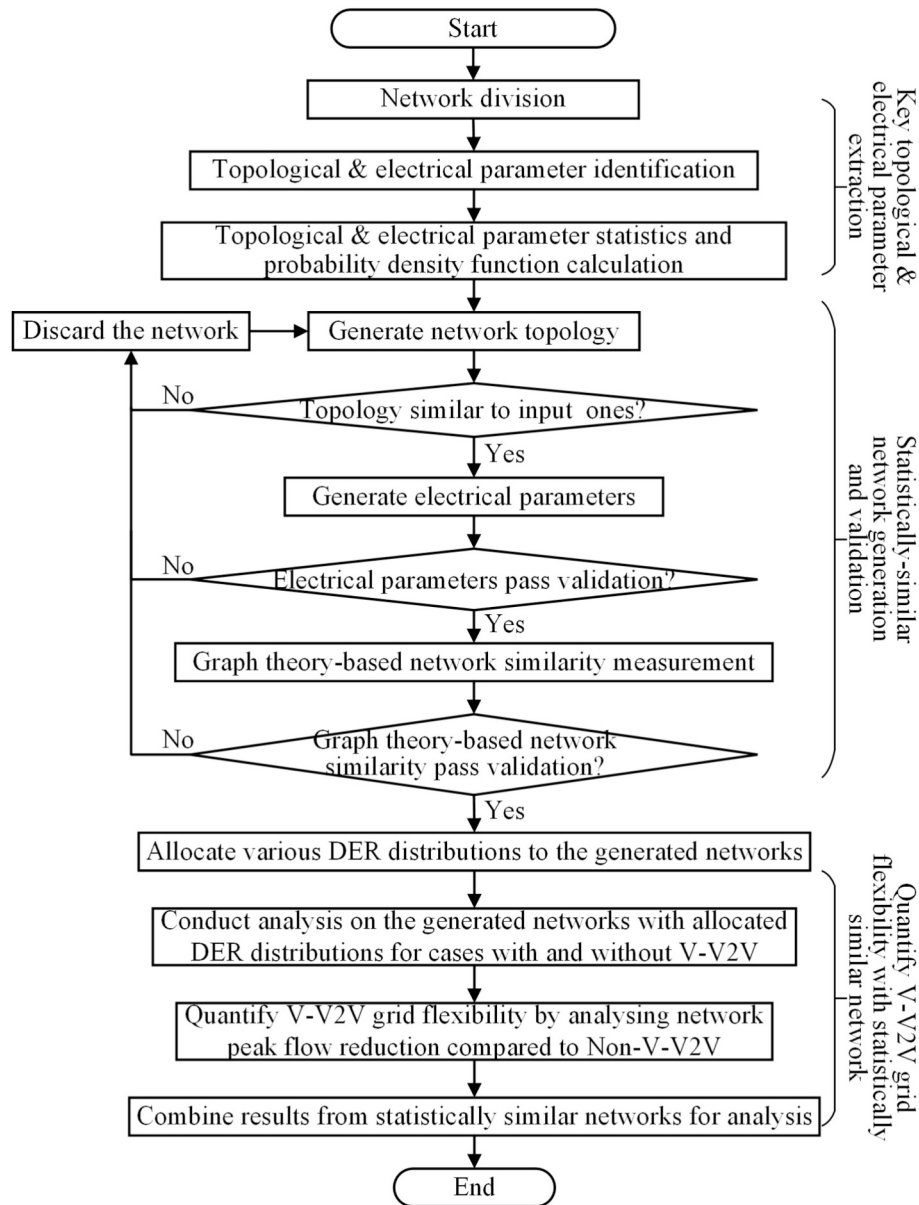


Fig. 5. Illustration of the quantification process based on the proposed statistically similar networks method.

both electrical and topological parameters, as well as their internal correlations. In addition to using a series of statistically similar networks, this study also considers the spatial randomness of EV user archetypes, PV installation capacities, and non-EV loads (including lighting, appliances, and heating/cooling loads) within the network, as well as the temporal randomness of loads and outputs across different days. Since the focus of this paper is on the impact of various EV charging modes on network power flows, flexibility from non-EV loads and household storage systems is not considered. The scenarios assume 100 % EV penetration, corresponding to the UK's 2050 net-zero goals.

Beyond different charging modes, the study also examines the differences in flexibility provision by V-V2V under various household charging power ratings (7 kW, 11 kW) and different plug-in habits ("graze charge" and "guzzle charge"). For graze charge, it is assumed that EV users will plug in when the SOC drops below 75 %, meaning they charge whenever the battery SOC is not very high. In contrast, guzzle charge assumes EV users only plug in when the SOC falls below 25 %, resulting in significantly shorter connection times. The key parameters of the EV user archetypes considered in this study, including battery

size, average annual electricity consumption, average percentage of EV potential availability time, and journey features, are listed in Table 1.

Four key metrics are defined to quantify the grid flexibility provision benefits of V-V2V: peak flow measurements for substations and power lines, annual APV, peak-to-average ratio, and annual electricity cost of all users. Peak flow measurements evaluate the impact of V-V2V on reducing peak demand across substations and different network levels, providing insights into how V-V2V mitigates loading constraints in the distribution system. Annual APV, mathematically defined in Section 4.5, represents the aggregated present value of asset costs, calculated based on the peak flow rate of substations and power lines relative to their capacity, offering a measure of the long-term financial and operational impact on the grid. Peak-to-average ratio captures the shape and smoothness of the load curve, indicating how effectively V-V2V redistributes charging demand to balance network utilization. Annual electricity cost of all users quantifies the direct financial impact of V-V2V on EV owners, highlighting potential cost savings. Together, these metrics provide a comprehensive evaluation of V-V2V's effectiveness in reducing network peak flows, increasing headroom capacity for

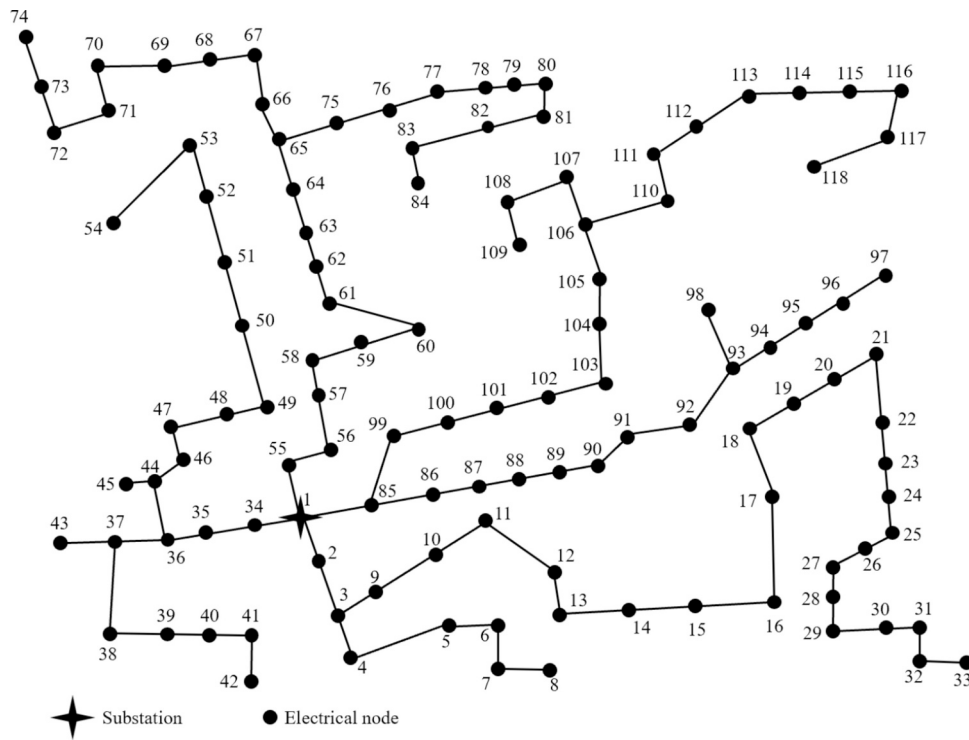


Fig. 6. Topology of the input network—a British 118-node low-voltage distribution network—used for the statistically similar networks method.

Table 1
Typical features of various EV user archetypes.

EV user archetypes	Battery size	Average annual electricity consumption (kWh)	Average percentage of EV potential availability time	Journey features	
One-EV household	<i>Ret-EV</i>	Medium	1700	80 %	Varied trips
One-EV household	<i>Pro-EV</i>	Medium	2200	50 %	No commuting
Two-EV household	<i>Sho-EV</i>	Small	2400	80 %	No long trips
Two-EV household	<i>Fam-EV</i>	Large	3100	80 %	No commuting

additional EVs, and delivering tangible economic benefits to EV users.

6.2. Charging curve generation for different EV user archetypes in base charging mode

In this section, charging curves for different EV user archetypes are generated in the base charging mode (Immediate Charge) based on the proposed bottom-up high-granularity EV travel and charging patterns modeling. Charging power is set to 7 kW and the plug-in pattern follows

the guzzle pattern (i.e., users charge less frequently, only when the SOC is relatively low, aligning with current EV user charging habits). Through simulation, Figs. 7–9 illustrate the charging curves for three types of EV users: One-EV household with *Pro-EV*, One-EV household with *Ret-EV*, and Two-EV households.

Specifically, Fig. 7 presents the generated EV charging curves for One-EV households with *Pro-EV*, illustrating the weekly charging patterns on an hourly timescale over several weeks. Each dashed curve in Fig. 7 represents the average value for all EVs, assuming the entire 118-

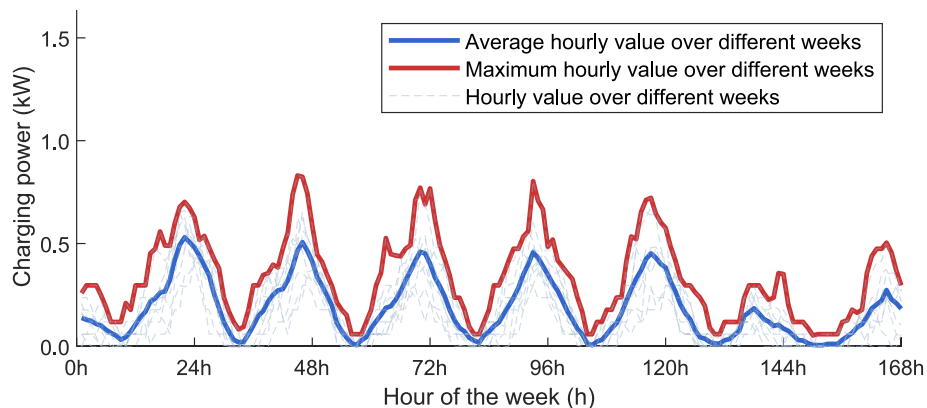


Fig. 7. Generated EV charging curves for one-EV households with *Pro-EV*, each representing the average for all EVs assuming the community consists of this EV user archetype.

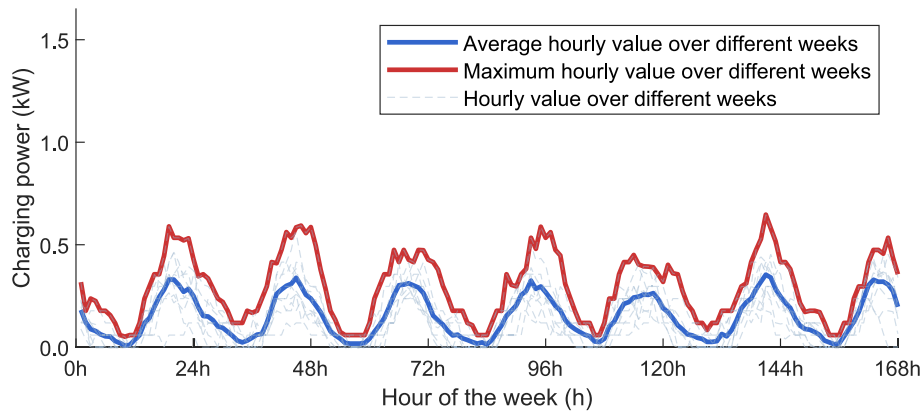


Fig. 8. Generated EV charging curves for one-EV households with *Ret-EV*, each representing the average for all EVs assuming the community consists of this EV user archetype.

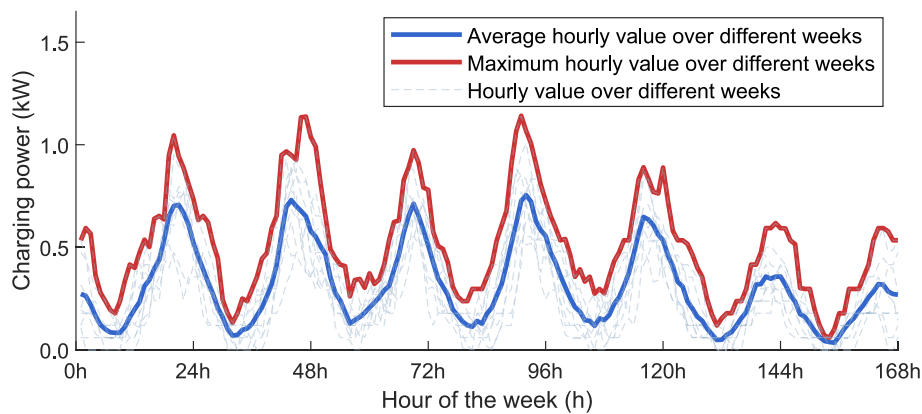


Fig. 9. Generated EV charging curves for Two-EV households, each representing the average for all EVs assuming the community consists of this EV user archetype.

node low-voltage distribution network consists solely of this user archetype. Here, the average hourly value, represented by the average of these dashed curves, is highlighted in blue, while the maximum hourly value curve is highlighted in red. Generally, the peak charging power for each weekday occurs around hour 21 or 22, while on weekends it typically falls between hours 19 and 23. The peak charging power across all days and weeks is approximately 0.83 kW, the highest value shown in the figure. It is evident that, compared to the peak power of an individual charger (with a rated power of 7 kW), the aggregated peak charging power per charger—at 0.83 kW for over a hundred vehicles in this distribution network—is significantly lower. However, this value is slightly higher than the peak per charger value observed in larger aggregations (tens of thousands or more EVs) on the National Grid, which is around 0.5 kW.

Similarly, Fig. 8 presents the generated EV charging curves for One-EV households with *Ret-EV*. The peak charging power for each day occurs between hours 19 and 23, with an overall peak across all days and weeks of approximately 0.65 kW, which is 22 % lower than the 0.83 kW peak of the *Pro-EV*. Notably, there are no significant differences between weekdays and weekends, as the travel patterns for *Ret-EV* users remain consistent. Fig. 9 shows the generated EV charging curves for Two-EV households with *Sho-EV* and *Fam-EV*. In this household type, where a single charger serves two EVs, the overall peak charging power across all days and weeks is approximately 1.14 kW—37 % higher than that of *Pro-EV* households and 75 % higher than *Ret-EV* households. Notably, the peak charging power during weekdays is also much higher than on weekends, with a weekend peak of 0.62 kW. The peak charging power for each day occurs between hours 19 and 23.

Overall, the peak charging power for One-EV households with *Pro-*

EV, One-EV households with *Ret-EV*, and Two-EV households with *Sho-EV* and *Fam-EV* is 0.83 kW, 0.65 kW, and 1.14 kW, respectively (representing the average per vehicle across approximately one hundred EVs aggregated in the 118-node distribution network). This highlights the differences in their peak values. Notably, while the total charging demand for Two-EV households (as shown in Table 1) may be 2–3 times higher than that of One-EV households, their peak charging power is only 1.4–1.8 times higher. This underscores the importance of detailed classification of EV user archetypes. Additionally, these households typically reach their peak charging power between hours 19 and 23 on weekdays, emphasizing the need for effective energy management and the importance of exploring new charging modes, which will be analyzed in detail in the next section.

6.3. Impact of V-V2V on network flow indicators and electricity costs across different charging habits and charger power ratings

This section presents a detailed analysis of the substation power flow under different charging modes, showing the weekly values on an hourly timescale for various networks. The results for different EV charger power ratings (7 kW and 11 kW) and different charging habits (graze charge and guzzle charge) are compared. Specifically, three scenarios were designed: Scenario I, where the EV charger power is set to 7 kW and charging habits follow the guzzle charge pattern; Scenario II, where the EV charger power is set to 11 kW with guzzle charge habits; and Scenario III, where the charger power is set to 7 kW and charging habits follow the graze charge pattern. As expected, higher-rated EV chargers allow for faster charging and stronger V2G capabilities, while graze charge habits lead to more frequent grid connection hours compared to

guzzle charge. Results and Impact comparison of different charging modes, charging habits, and charger power on network flow indicators and electricity costs are illustrated in Table 2 and Figs. 10–12.

In all three scenarios, immediate charge results in the highest peak substation flow compared to the other charging modes (Smart Charge, V2G, V-V2V). Specifically, both Smart Charge and V2G slightly reduce the peak flow relative to Immediate Charge. For example, in Scenario I, the peak substation flow decreases from 164 kW to 137 kW with Smart Charge and to 135 kW with V2G. Notably, although V2G unlocks additional flexibility by allowing EVs to discharge back to the grid, the network flow—both the peak flow at substations and power lines, and the annual APV, which captures the combined peak flow of substations and power lines—does not show a significant reduction compared to Smart Charge. In fact, in Scenario III, the peak substation flow increases from 137 kW to 146 kW with V2G. This occurs because, without a proper mechanism (or when influenced solely by time-of-use pricing), EV users tend to leverage V2G primarily for cost-saving arbitrage rather than for reducing network peak flows. For example, in Scenario III, V2G reduces annual energy costs from £157.4 k to £145.4 k, but this does not necessarily help mitigate peak network flow. Instead, it can create new peaks during low-price periods (traditionally low-load times), as illustrated in Fig. 12, where the peak load in V2G is delayed by several hours compared to Smart Charge. While high-price period loads are reduced, the delayed peak load is even higher.

Unlike V2G, V-V2V not only allows EVs to discharge back to the grid, but also enables virtual energy sharing between EVs through the distribution network. This includes sharing between home-charged and public-charged EVs of the same type, as well as between different types of EVs. In this framework, the charging and discharging management of EVs is not solely based on individual cost minimization. Instead, it considers the collective benefit of all EV users connected to the same distribution network while also taking into account network peak flow indicators (such as the APV metric used in this study). The goal is to optimize overall electricity costs while reducing peak flow, thereby potentially alleviating network capacity pressures. As shown in Table 2 and Figs. 10–11, V-V2V achieves the lowest peak substation flow compared to the other three charging modes across all scenarios (I, II, and III). Correspondingly, it also has the lowest peak-to-average ratios and APV values. Additionally, V-V2V significantly reduces electricity costs compared to the other charging modes, making it a win-win solution for both EV users and network operators.

Notably, the flexibility improvement brought by V-V2V to the distribution network—such as reducing peak flow and lowering electricity costs—is influenced to varying degrees by charger power ratings and EV

user charging habits. Charger power ratings have a modest impact on V-V2V's ability to provide flexibility. For example, in Scenario II compared to Scenario I, V-V2V shows slight improvements in peak substation flow, peak-to-average ratio, and annual APV, indicating better network performance with smaller values. Additionally, there is a small reduction in annual electricity costs.

However, the impact of EV user charging habits is much more pronounced. Both Scenario I and Scenario III have the same charger power rating of 7 kW, but in Scenario III, EV users follow the graze charge habit, where they are more willing to connect to the grid even when the SOC is relatively high. Under V-V2V in Scenario III, the substation peak flow decreases from 118 kW to 93 kW, a reduction of 21 % compared to Scenario I. Furthermore, V-V2V in Scenario III reduces substation peak flow by 36 % compared to V2G in the same scenario, where the peak flow is 146 kW. As shown in Fig. 12, the peak flow curve under V-V2V in Scenario III is much smoother, with no significant spikes, and the peak-to-average ratio is reduced to 121 %, demonstrating V-V2V's excellent ability to reduce network peak flow. Moreover, Scenario III also shows the greatest reduction in electricity costs. This indicates that in the future, as EV user charging habits shift toward graze charge—where users frequently connect their EVs to chargers, such as plugging in daily after returning home—V-V2V will play a significant role in reducing both network peak flow and electricity costs. Even under current EV user habits, where users only connect to the grid when SOC falls below a low threshold (e.g., 25 %), V-V2V's flexibility capabilities are still clearly demonstrated, as seen in Table 2 and Figs. 10–11.

6.4. Spatio-temporal analysis of V-V2V impact on power line flows across different levels of the low-voltage distribution network

The previous section demonstrated the impact of V-V2V on substation peak flow, including a detailed analysis of substation flow on an hourly timescale over a week. This sub-section presents a spatio-temporal analysis of V-V2V's impact on peak power line flows across different levels of the low-voltage distribution network, examining how V-V2V affects power line flows at various network levels. The results are presented in Table 3 and Figs. 13–16. Specifically, the average value of power line peak flow at different network levels under various charging modes is shown in Table 3. First, the impact of different charging modes on power line peak flows across the network levels is similar to the impact on substation peak flow, as discussed in subsection 6.3. That is, Smart Charge and V2G show minimal reduction in peak flow, whereas V-V2V has a significant effect across all network levels. For the near-substation level (Level 1), V-V2V reduces the average peak flow of power lines by 57 %. At the intermediate level (Level 2), the reduction is also 57 %, while at the near-terminal user level (Level 3), V-V2V reduces peak flow by 55 %. This demonstrates that the flexibility provided by V-V2V in reducing power line peak flow is comprehensive, greatly alleviating capacity pressures across all parts of the network.

Figs. 13–16 show the average hourly power line flow at each network level for a typical day under four charging modes: Immediate Charge, Smart Charge, V2G, and V-V2V. It is evident that moving from Immediate Charge to Smart Charge (or V2G), the power line peak flow at different network levels decreases slightly. Although V2G shows a slightly higher peak flow compared to Smart Charge, this is due to larger peaks during low-price hours. V-V2V, without a doubt, results in the lowest peak flows. Its hourly power line flow curve is much smoother across all network levels, with minimal differences in flow between hours and no sharp peaks. Additionally, during high-price hours, a valley in power line flow is observed due to coordinated EV discharging. Overall, these figures further demonstrate the effectiveness of V-V2V in reducing peak flows of power lines across the entire network, regardless of their position within the network levels.

Table 2
Impact of charging modes on network flow indicators and electricity cost.

Scenarios	Charging mode	Peak substation flow (kW)	Peak-to-average ratio (%)	Annual APV (k £)	Annual electricity cost (k£)
Scenario I	Immediate Charge	164	229 %	12.1	163.2
	Smart Charge	137	192 %	8.5	156.6
	V2G	135	188 %	8.8	155.4
	V-V2V	118	164 %	5.3	146.3
Scenario II	Immediate Charge	169	236 %	13.8	164.3
	Smart Charge	137	192 %	9.4	156.5
	V2G	134	188 %	10.2	155.3
	V-V2V	110	152 %	5.2	143.9
Scenario III	Immediate Charge	164	229 %	12.0	164.1
	Smart Charge	137	192 %	8.5	157.4
	V2G	146	201 %	10.7	145.4
	V-V2V	93	121 %	2.1	124.5

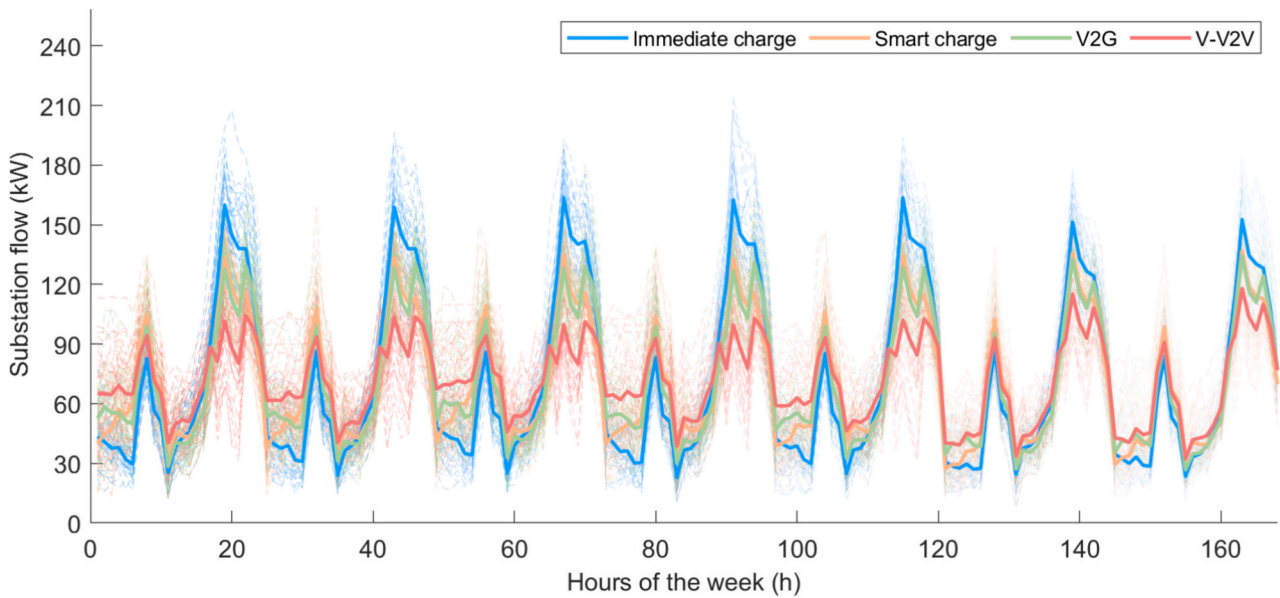


Fig. 10. Substation power flow comparison for different charging modes in Scenario I.

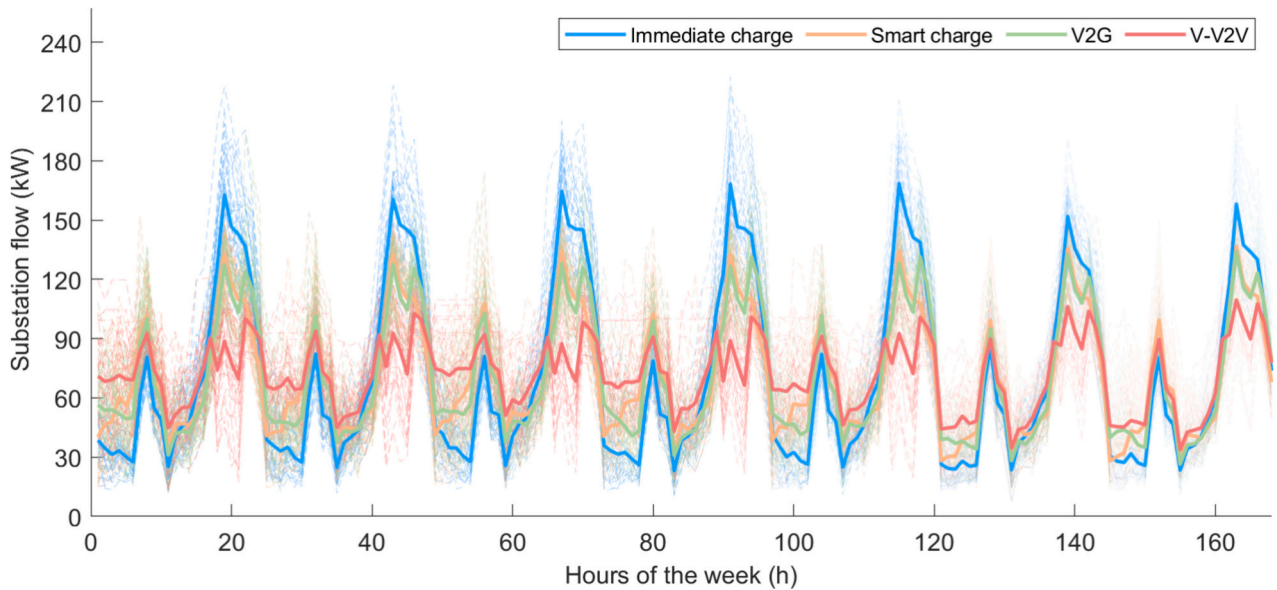


Fig. 11. Substation power flow comparison for different charging modes in Scenario II.

7. Conclusions

This paper proposes the V-V2V framework, enabling EVs to share energy with each other, whether at public charging stations or home, as long as they are connected to the same distribution network. The framework eliminates the need for physical proximity and peer-to-peer matching seen in traditional V2V, enhancing grid flexibility and reducing capacity pressures by harmonizing EV charging with other demands and photovoltaic generation. To quantify the benefits of V-V2V framework's flexibility provision in reducing network peak flows, this paper implements and enhances the statistically similar networks method, where simulations are based on generated networks that share similar electrical and topological characteristics, rather than relying on a single network. Using graph theory, the method preserves statistical similarity in both electrical and topological features, along with their internal correlations, ensuring the practicality of the network simulations. To improve flexibility quantification accuracy, this paper

introduces a bottom-up, high-granularity model of EV travel and plugging patterns that accounts for diverse user archetypes. Monte Carlo simulations are employed to provide a detailed analysis of travel and charging behaviors by categorizing EV users. The effectiveness of the proposed method is tested through numerical results using real-world UK distribution networks.

The results show that V-V2V consistently achieves the lowest peak substation flow compared to the other three charging modes across all scenarios, regardless of charger rated power and charging habits, with network peak flow reductions of up to 36 % compared to the non-V-V2V case (e.g., V2G charging modes). It also exhibits the lowest peak-to-average ratios and asset's present values, with the latter showing a reduction of up to 80 %. Moreover, V-V2V significantly reduces electricity costs relative to other charging modes, with savings ranging from 6 % to 14 % compared to the non-V-V2V case, offering a mutually beneficial solution for both EV users and network operators. As charging habits shift toward "graze charge", where users frequently connect their

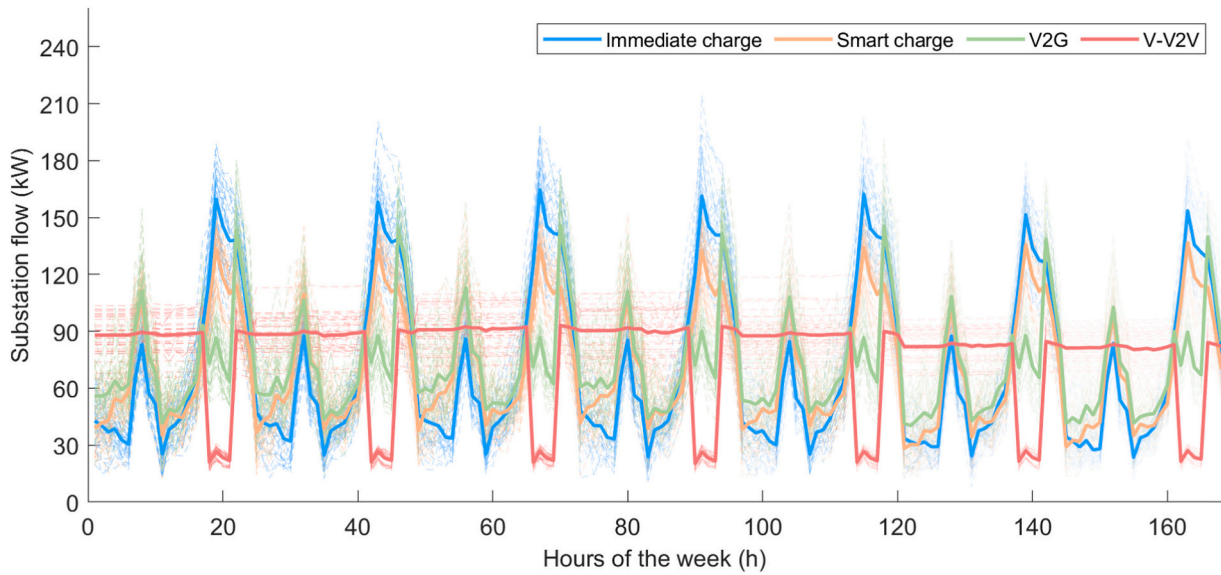


Fig. 12. Substation power flow comparison for different charging modes in Scenario III.

Table 3

Average value of power line peak flow at different network levels under various charging modes.

Average value of peak flow of power lines at each network level (kW)	Immediate Charge	Smart Charge	V2G	V-V2V
Near-substation level (level 1)	28.8	25.4	28.4	12.5
Intermediate level (level 2)	16.9	15.7	17.8	7.2
Near-terminal user level (level 3)	10.7	10.3	11.9	4.8

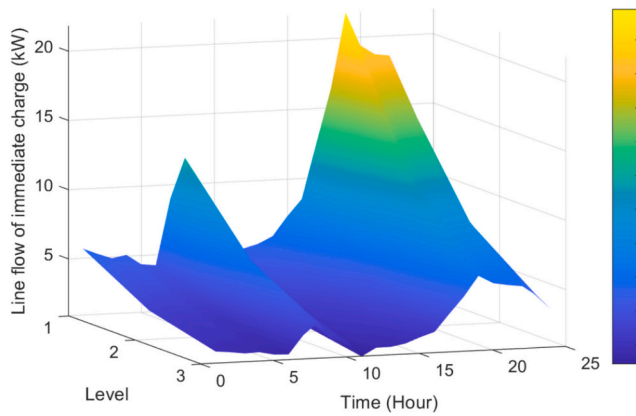


Fig. 13. Average hourly power line flow at each network level for a typical day (immediate charge).

EVs to chargers (such as daily plugging in after returning home), V-V2V will play an increasingly crucial role in lowering both network peak flows and electricity costs. Overall, these results highlight the effectiveness of V-V2V in reducing peak line flows across the entire network, regardless of the specific network level.

While this study focuses on validating the V-V2V framework within local distribution networks, future research could explore the scalability of the proposed method to higher-level power networks for V-V2V sharing. Scaling the framework to a broader level would require incorporating the spatiotemporal locations of EV users' trips and accounting for charging and V-V2V activities beyond home charging, such as at offices, commercial districts, and other public locations. Additionally,

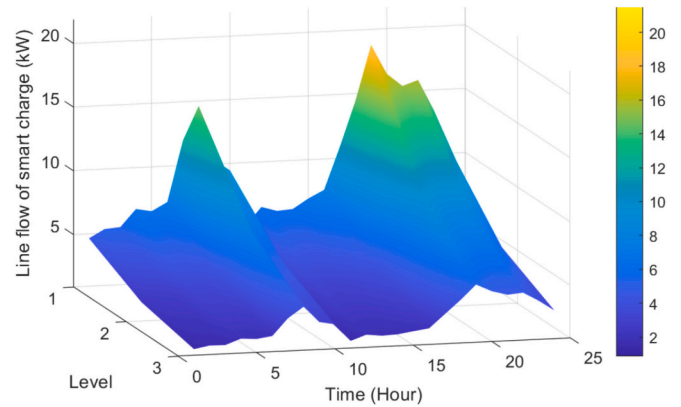


Fig. 14. Average hourly power line flow at each network level for a typical day (smart charge).

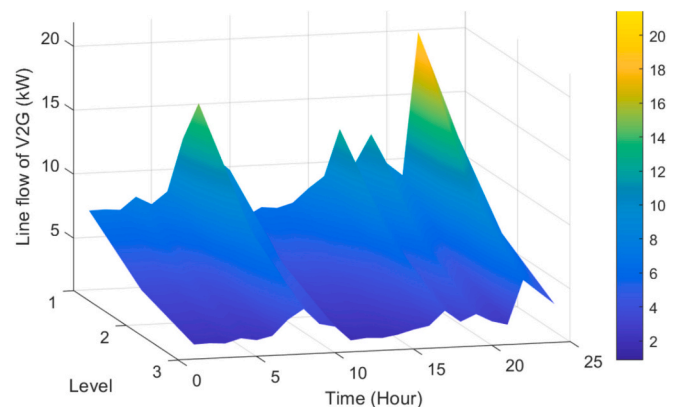


Fig. 15. Average hourly power line flow at each network level for a typical day (V2G).

expanding the framework would require further investigation into the modeling of larger networks and their key components, as well as refinements to the statistically similar network-based method to better accommodate meshed transmission structures. Additionally, future

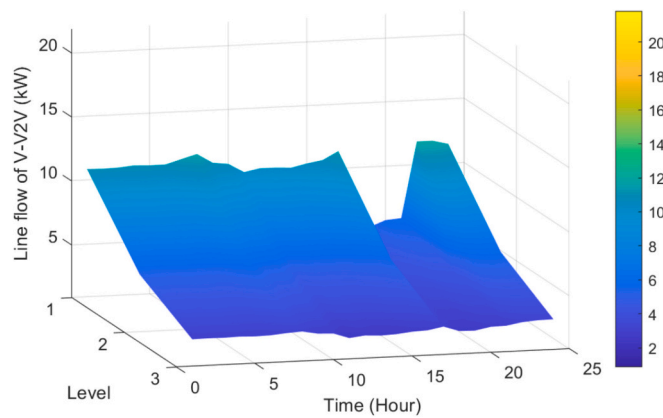


Fig. 16. Average hourly power line flow at each network level for a typical day (V-V2V).

work will further refine the analysis of V-V2V implementation, particularly in terms of ensuring sufficient EV energy availability and driving safety. This is especially critical as users may have unexpected long-distance travel needs, yet their EVs might lack sufficient charge due to prior participation in V-V2V energy sharing. Addressing these practical concerns will be essential for facilitating the real-world adoption of V-V2V, ensuring an effective balance between grid flexibility and individual travel needs.

CRedit authorship contribution statement

Wei Gan: Writing – original draft, Validation, Software, Methodology, Investigation. **Yue Zhou:** Writing – review & editing, Supervision, Investigation, Conceptualization. **Jianzhong Wu:** Writing – review & editing, Supervision, Project administration, Funding acquisition.

Declaration of competing interest

The authors declare that they have no known competing financial interests or personal relationships that could have appeared to influence the work reported in this paper.

Acknowledgements

This research was funded by the UK's Engineering and Physical Sciences Research Council under Grant EP/Y016114/1 (Supergen Energy Networks Impact Hub).

Data availability

Data will be made available on request.

References

- [1] Tian X, An C, Chen Z. The role of clean energy in achieving decarbonization of electricity generation, transportation, and heating sectors by 2050: a meta-analysis review. *Appl Energy* 2023;182:113404.
- [2] Capuder T, Sprčić DM, Zoričić D, Pandžić H. Review of challenges and assessment of electric vehicles integration policy goals: integrated risk analysis approach. *Int J Electr Power Energy Syst* 2020;119:105894.
- [3] Husain I, Ozpineci B, Islam MS, Gurpinar E, Su GJ, Yu W, et al. Electric drive technology trends, challenges, and opportunities for future electric vehicles. *Proc IEEE* 2021;109(6):1039–59.
- [4] Li L, Wang Z, Chen L, Wang Z. Consumer preferences for battery electric vehicles: a choice experimental survey in China. *Transp Res Part D: Transp Environ* 2020;78:102185.

- [5] National Energy System Operator. Future Energy Scenarios 2024: ESO Pathways to Net Zero, <https://www.neso.energy/document/321041/download> (accessed 9 August 2024).
- [6] IEA, Global EV Outlook 2024: Moving towards increased affordability, <https://www.iea.org/reports/global-ev-outlook-2024> (accessed 9 August 2024).
- [7] Das HS, Rahman SA, Tan CW, Yatim AHM. Electric vehicles standards, charging infrastructure, and impact on grid integration: a technological review. *Renew Sust Energy Rev* 2020;120:109618.
- [8] Damianakis N, Mouli GRC, Bauer P, Yu Y. Assessing the grid impact of electric vehicles, heat pumps & PV generation in Dutch LV distribution grids. *Appl Energy* 2023;352:121878.
- [9] Fachrizal R, Ramadhani UH, Munkhammar J, Widén J. Combined PV–EV hosting capacity assessment for a residential LV distribution grid with smart EV charging and PV curtailment. *Sustain Energy Grids Netw* 2021;26:100445.
- [10] Manríquez F, Sauma E, Aguado J, de la Torre S, Contreras J. The impact of electric vehicle charging schemes in power system expansion planning. *Appl Energy* 2020;262:114527.
- [11] Heuberger CF, Bains PK, Mac Dowell N. The EV-olution of the power system: a spatio-temporal optimisation model to investigate the impact of electric vehicle deployment. *Appl Energy* 2020;257:113715.
- [12] Ghazvini MAF, Verzijlbergh RA, Wedephol DB, Slootweg H. Congestion management in active distribution networks through demand response implementation. *Sustain Energy Grids Netw* 2019;17:100185.
- [13] Pan H, Feng X, Li F, Yang J. Energy coordinated control of DC microgrid integrated incorporating PV, energy storage and EV charging. *Appl Energy* 2023;342:121155.
- [14] Wang L, Dubej A, Gebremedhin AH, Srivastava AK, Schulz N. MPC-based decentralized voltage control in power distribution systems with EV and PV coordination. *IEEE Trans Smart Grid* 2022;13(4):2908–19.
- [15] Electric vehicle energy tariffs. What are they and how do they work? <https://www.moneysavingexpert.com/utilities/ev-energy-tariffs/> (accessed 9 August 2024)
- [16] How EV tariffs work for electric cars, <https://octopusenergy.com/ev-hub/guide-to-energy-tariffs-for-electric-cars> (accessed 9 August 2024).
- [17] Upputuri RP, Subudhi B. A comprehensive review and performance evaluation of bidirectional charger topologies for V2G/G2V operations in EV applications. *IEEE Trans Transp Electrification* 2023;10(1):583–95.
- [18] Singh K, Singh A. Behavioural modelling for personal and societal benefits of V2G/V2H integration on EV adoption. *Appl Energy* 2022;319:119265.
- [19] Gunkel PA, Bergaentzle C, Jensen IG, Scheller F. From passive to active: flexibility from electric vehicles in the context of transmission system development. *Appl Energy* 2020;277:115526.
- [20] Zhang J, Che L, Wan X, Shahidehpour M. Distributed hierarchical coordination of networked charging stations based on peer-to-peer trading and EV charging flexibility quantification. *IEEE Trans Power Syst* 2021;37(4):2961–75.
- [21] Wei H, Zhang Y, Wang Y, Hua W, Jing R, Zhou Y. Planning integrated energy systems coupling V2G as a flexible storage. *Energy* 2022;239:122215.
- [22] Hannan MA, Mollik MS, Al-Shetwi AQ, Rahman SA, Mansor M, Begum RA, et al. Vehicle to grid connected technologies and charging strategies: operation, control, issues and recommendations. *J Clean Prod* 2022;339:130587.
- [23] İnci M, Savrun MM, Çelik Ö. Integrating electric vehicles as virtual power plants: a comprehensive review on vehicle-to-grid (V2G) concepts, interface topologies, marketing and future prospects. *J Energy Storage* 2022;55:105579.
- [24] Li X, Xiang Y, Lyu L, Ji C, Zhang Q, Teng F, et al. Price incentive-based charging navigation strategy for electric vehicles. *IEEE Trans Ind Appl* 2020;56(5):5762–74.
- [25] Whitehead J, Washington SP, Franklin JP. The impact of different incentive policies on hybrid electric vehicle demand and price: An international comparison. *World Electr Veh J* 2019;10(2):20.
- [26] Wang H, Jia Y, Shi M, Xie P, Lai CS, Li K. A hybrid incentive program for managing electric vehicle charging flexibility. *IEEE Trans Smart Grid* 2022;14(1):476–88.
- [27] Liu C, Chau KT, Wu D, Gao S. Opportunities and challenges of vehicle-to-home, vehicle-to-vehicle, and vehicle-to-grid technologies. *Proc IEEE* 2013;101(11):2409–27.
- [28] Dhungana A, Bulut E. Peer-to-peer energy sharing in mobile networks: applications, challenges, and open problems. *Ad Hoc Netw* 2020;97:102029.
- [29] Shurrab M, Bahabry A, Boukerche A, Cherkaoui S, Ramadan A, Lakas A. An efficient vehicle-to-vehicle (V2V) energy sharing framework. *IEEE Internet Things J* 2021;9(7):5315–28.
- [30] Koufakis AM, Loukarakis E, Saberi S, Shokri-Ghadikolaei H, Vasilakos AV. Towards an optimal EV charging scheduling scheme with V2G and V2V energy transfer. In: 2016 IEEE Int Conf smart grid Commun (SmartGridComm). IEEE; 2016.
- [31] Cenex. Project Sciurus Trial Insights: Findings from 300 Domestic V2G Units in 2020. Available, <https://www.cenex.co.uk/app/uploads/2021/05/Sciurus-Trial-Insights.pdf> (accessed 9 Aug 2024).
- [32] National Travel Survey. Technical report. <https://www.gov.uk/government/statistics/national-travel-survey-2022-technical-report>; 2022 (accessed 9 August 2024).
- [33] Wei W, Wu L, Wang J, Mei S. Expansion planning of urban electrified transportation networks: a mixed-integer convex programming approach. *IEEE Trans Transp Electrification* 2017;3(1):210–24.
- [34] Gan W, Shahidehpour M, Guo J, Yao W, Pandey S, Paaso EA, et al. A tri-level planning approach to resilient expansion and hardening of coupled power distribution and transportation systems. *IEEE Trans Power Syst* 2021;37(2):1495–507.